

This is an Open Access document downloaded from ORCA, Cardiff University's institutional repository: <https://orca.cardiff.ac.uk/id/eprint/129651/>

This is the author's version of a work that was submitted to / accepted for publication.

Citation for final published version:

Bonilla-Villalba, Pedro, Claus, Susanne, Kundu, Abhishek and Kerfriden, Pierre 2020. Goal-oriented model adaptivity in stochastic elastodynamics: simultaneous control of discretisation, surrogate model and sampling errors. *International Journal for Uncertainty Quantification* 10 (3) , pp. 195-223.
10.1615/Int.J.UncertaintyQuantification.2020031735

Publishers page: <http://dx.doi.org/10.1615/Int.J.UncertaintyQuantif...>

Please note:

Changes made as a result of publishing processes such as copy-editing, formatting and page numbers may not be reflected in this version. For the definitive version of this publication, please refer to the published source. You are advised to consult the publisher's version if you wish to cite this paper.

This version is being made available in accordance with publisher policies. See <http://orca.cf.ac.uk/policies.html> for usage policies. Copyright and moral rights for publications made available in ORCA are retained by the copyright holders.



Goal-oriented model adaptivity in stochastic elastodynamics: simultaneous control of discretisation, surrogate model and sampling errors

Pedro Bonilla-Villalba^{*1}, Susanne Claus², Abhishek Kundu¹, and
Pierre Kerfriden^{1,3}

¹Institute of Mechanics Materials and Advanced Manufacturing
Cardiff University, CF24 3AA, United Kingdom

^{*}e-mail: bonilla-villalbap@cardiff.ac.uk

²ONERA, 6 Chemin de la Vauve aux Granges, 91120 Palaiseau, France

³Centre des Matériaux, MINES ParisTech / PSL University, 63-65 rue Henri Auguste
Desbruères, Corbeil-essonne, France

February 2020

Abstract

The presented adaptive modelling approach aims to jointly control the level of refinement for each of the building-blocks employed in a typical chain of finite element approximations for stochastically parametrized systems, namely: (i) finite error approximation of the spatial fields (ii) surrogate modelling to interpolate quantities of interest(s) in the parameter domain and (iii) Monte-Carlo sampling of associated probability distribution(s). The control strategy seeks accurate calculation of any statistical measure of the distributions at minimum cost, given an acceptable margin of error as only tunable parameter. At each stage of the greedy-based algorithm for spatial discretisation, the mesh is selectively refined in the subdomains with highest contribution to the error in the desired measure. The strictly incremental complexity of the surrogate model is controlled by enforcing preponderant discretisation error integrated across the parameter domain. Finally, the number of Monte-Carlo samples is chosen such that either (a) the overall precision of the chain of approximations can be ascertained with sufficient confidence, or (b) the fact that the computational model requires further mesh refinement is statistically established. The efficiency of the proposed approach is discussed for a frequency-domain vibration structural dynamics problem with forward uncertainty propagation. Results show that locally adapted finite element solutions converge faster than those obtained using uniformly refined grids.

Keywords: Adaptivity; Stochastic Control and Estimation; Stochastic finite element method; Solid mechanics

1 Introduction

Solving partial differential equations with uncertain parameters requires large amount of computational resources. This is due not only to the potential complexity of the numerical model (in our case finite elements - FEM) but also to the vast quantities of evaluations of the numerical model required to capture the probability density function of the output quantity of interest (QoI).

In order to reduce this computational burden, we may act at three different levels. Firstly, mesh refinement should be done only where it significantly contributes to increasing the accuracy of the predicted QoI. Secondly, surrogate modelling may be used to take advantage of a potential “offline/online”

^{*}Corresponding author

split of the overall numerical complexity. Finally, we may attempt to reduce the number of Monte-Carlo (MC) iterations. In this paper, we developed an algorithmic technology to control these three levels of numerical refinement together, in a goal-oriented manner.

Adaptive mesh refinement is a well known approach to optimise computational resources in finite element technologies [1, 2]. Typically, a posteriori error indicators are used to guide the refinement process. Regarding uncertainty quantification (UQ), non-probabilistic approaches bound the risk (*e.g.* fuzzy arithmetic methods [3] or worst-case-scenario [4]) while probabilistic approaches describe the likelihood of the complete range of possible outcomes. The latter category is relevant in this work, and more specifically methods that rely on adequately sampling the parameter space.

On the one hand, researchers working in the area of finite element model verification traditionally focus on quantifying and controlling spatial discretisation errors specifically [5, 6, 7]. On the other hand, researchers in numerical methods for probabilistic PDEs are usually more interested in the reduction of the sampling error [8, 9, 10], in the development of surrogate models [11, 12, 13, 14, 15] or in the reduction of the number of relevant parameters [16, 17, 18]. More recently [19] uses error estimation to enrich locally a model surrogate (without controlling the FE discretisation per se).

There exist some directions of research to control or reduce the cost of this combination of errors, including (i) the bounding of UQ error separately and sensitivity analysis on the discretisation bound [20, 21, 22], (ii) the extension of goal-oriented error estimators to stochastic frameworks to obtain bounds [23, 24, 25, 26, 27] which allows reduction of the predominant error at each stage although not under a single criterion and without considering the effect of local mesh refinement on the stochastic process (iii) adaptivity to describe an embedded surface which does not have uncertainty propagation [28], (iv) adaptivity of errors based in the Arlequin method considering uniform refinement to reduce the discretisation error [29] (and requiring a fine enough mesh to perform stochastic evaluations), and (v) optimisation of the hierarchy of meshes used in the framework of Multi Level Monte Carlo methods (see [30]) in order to reduce the sampling cost of evaluating the finer mesh [31].

Yet, only in the framework of the Stochastic Finite Element Method (stochastic process at element level) an optimal empiric relation between the mesh size and the stochastic characterisation has been studied [32, 33, 34]. Furthermore, none of the previous works explores how local mesh adaptivity affects the stochastic error. To the authors knowledge the latter has solely been explored in [35] within the framework of Multi-Level Monte Carlo. It is the purpose of the present paper to delve into this relation with the stochastic processes out of the finite element and in a single mesh framework, so that all approaches can benefit from it.

Specifically, an algorithm is proposed to minimise the computational cost of adaptively reducing the error of any QoI due to discretisation until it is on the same scale as the forwarded uncertainty of any desired probabilistic measure of this QoI (expectation or percentile in this work), which is an unknown dependent random variable. The novel approach is as follows. Optimality is pursued by refining the spatial discretisation greedily and locally, whilst incrementally increasing the surrogate model. Each refined solution is then compared to the uncertainty through a non-dimensional precision parameter representing the exact proportion of the errors the user is willing to accept (see equation 29). The spatial error contribution is simply estimated by refining the polynomial order of the finite element mesh, and using the adjoint methodology to propagate the effect of local errors to the QoI. The contribution of the surrogate model is evaluated directly, at sampling points of the parameter domain. Subsequently, we force the reduced model to be such that it produces a response surface whose error contributions are similar in amplitude than the surface obtained from the discrete FEM model. Finally, the MC sampling is performed adaptively. It is stopped when either (i) the QoI is computed with a sufficiently low level of error or (ii) we are sufficiently confident that the desired level of precision cannot be achieved with the current combination of mesh and surrogate model, which indicates need of further local refinement. We believe that this simplicity is attractive in terms of engineering practices.

This paper follows up chapter 5 of the doctoral thesis [36]. The thesis included the algorithm and results for the expectation of a single QoI, expanded here to any probabilistic measure and QoI (with additional results for percentiles and strains with respect to the expectation of the displacement). It is organised as follows. Section 2 consists on a quick reference table of notation to improve readability.

ity. Afterwards, formal notation and equations are introduced in detail, being section 3 devoted to parametrised finite element problems in elastodynamics and section 4 to the stochastic formulation and reduced order model. The latter section contains also a first discussion regarding the various sources of numerical errors of the whole posed problem (sub-section 4.3). In section 5, the interactions between these errors are investigated numerically. We also introduce the adaptive algorithm for the approximation scheme outlined previously. Finally, section 6 displays and discusses results with the aim to verify that the algorithm controls all different sources of error.

2 Table of notation

This section contains the most important symbols used as notation in the paper for quick reference.

Boundary valued problem notation	
$\mathbf{x} ; t$	Spatial and time coordinates
$\vec{n} ; \vec{e}_y$	Unit vector normal to the boundary; unit vector following Cartesian axis y
$\nabla_s ; Tr(\bullet)$	Symmetric gradient; trace of \bullet
\mathbb{I}	Identity tensor of adequate size
$\Omega ; \Omega_k ; \partial\Omega$	Domain ; domain of the element e_k ; and Boundary
$\Gamma_d ; \Gamma_n$	Subset of the boundary where Dirichlet and Neumann prescribed values are applied
u	Displacement field, solution to the vibration problem
v	Continuous test field used in the weak formulation
e	Error in the displacement
ϵ	Error in a quantity of interest. Specific errors in quantities of errors are : $\epsilon_{/}$ relative, ϵ_σ normalised by the standard deviation, ϵ_{NM} of the numerical model, ϵ_{PC} due to polynomial chaos
ε	Estimation of an error or tolerance for an error
$a^\omega(\cdot, \cdot)$	Bilinear form of the vibrating structure problem under a harmonic load (eq. 4)
$l(\cdot)$	Right hand side of the weak problem including source/forcing function & prescribed BC terms
$f(\cdot) ; F(\cdot)$	Source or forcing function. Capital for time dependent version
$u_d(\cdot) ; U_d(\cdot)$	Prescribed Dirichlet boundary data. Capital for time dependent version
$g_n(\cdot) ; G_n(\cdot)$	Prescribed Neumann boundary data. Capital for time dependent version
$\mathcal{R}^\omega(\bullet)$	Residual of field \bullet related to the vibrating structure problem (examples eq. 13 17 18)
$E(\mathbf{x}, \boldsymbol{\mu})$	Parametric Young's moduli (see stochastic symbols for the parameter $\boldsymbol{\mu}$)
$C(E(\mathbf{x}, \boldsymbol{\mu}), \nu)$	Fourth order Hooke tensor (function of the parametric Young's moduli an Poisson ratio)
ω	Circular frequency for the load
Finite element method notation	
\mathcal{L}^p	Lesbesgue functional space with finite p-norms
\mathcal{H}^o	Sobolev space which contains \mathcal{L}^2 functions whose weak derivatives up to order o are also \mathcal{L}^2
\mathcal{U}	Space of continuous solutions to the problem posed
\mathcal{V}	Space of trial solutions equalling zero at the Dirichlet boundary
$\mathcal{V}^h ; \hat{\mathcal{V}} ; \tilde{\mathcal{V}}$	Coarse; refined (rich); and reference or last computable piece-wise discrete spaces of trial functions. Notation extended to solution spaces, meshes, shape functions, solution and error fields, estimators and indicators related with the corresponding discretisation
$\mathcal{M} ; m$	Mesh defining a discretisation; index identifying a mesh
h	Characteristic radius of the circumscribed circle of the elements of a FE mesh. As a super-index determines the discrete coarse version of a space, field, mesh, shape function, estimator or indicator

$\mathfrak{e}; \mathbb{k}$	Finite element forming a mesh; index identifying an element of the mesh
$\psi^{\mathfrak{h}}; \widehat{\psi}$	Shape functions, coarse and fine versions. In this paper it is either order 1 and 2 polynomials for a given mesh, or both sets of order 1 polynomials determined by the initial and the refined mesh.
$[u^{\mathfrak{h}}]$	Vector of coefficients of a field. Field $u^{\mathfrak{h}}$ can be reproduced as $[u^{\mathfrak{h}}] \cdot \psi^{\mathfrak{h}}$
$\mathcal{V}^{\mathfrak{h}}$ π $\widehat{\mathcal{V}}$	Projector operator from a rich to a coarse field (see eq. 35)

Error control notation

$\eta^{type}; \eta_{\mathbb{k}}^{type}$	Global error estimator; indicator of refinement of type ' <i>type</i> ' for the element $\mathfrak{e}_{\mathbb{k}}$
MN;EN;D; \perp	Types of η . Mass norm; energy norm; localised QoI; orthogonal localised QoI;
δ	and QoI localised extracting the projection to the coarse FE space
$q(\cdot)$	Function mapping from the solution to a quantity of interest
z	Influence field or influence function (reflects influence of the residual upon the QoI, eq. 18)

Stochastic process notation

$\boldsymbol{\mu}$	Primary random variable vector of r real parameters influencing $C(\mathbf{x}, \boldsymbol{\mu})$ (eq. 8)
Q	Response or forwarded random variable result of applying $q()$ to the all solutions $u(\mathbf{x}, \boldsymbol{\mu})$
$\mathfrak{M}()$	Numerical FEM model. It maps from the primary known random variable(s) $\boldsymbol{\mu}$ to the unknown stochastic forwarded one function of it(them) Q
$s; s'$	Sub-indexes identifying a sampling point and a control point
$\Theta; \Theta_Q$	Sampling spaces of the primary and response stochastic processes
\mathcal{F}	Smallest σ -algebra consisting of a set of all measurable subsets
$f_{\boldsymbol{\mu}}^{\mathcal{P}}; f_Q^{\mathcal{P}}$	Probability density function of the sub-indexed random variable
$\theta_s; Q_s$	Outcomes of the random variables $\boldsymbol{\mu}$ and Q respectively for sample s
$\mathcal{U}(1,2)$	Uniform distribution in the interval [1,2]
$\mathcal{N}(1,2)$	Normal distribution with mean 1 and variance 2
$std(\bullet); \sigma$	Standard deviation of \bullet
$\mathcal{E}[\bullet]; \overline{\mathcal{E}}[\bullet]$	Expectation of \bullet ; its discrete Monte Carlo approximation (eq. 20; 21)
$\mathcal{C}_{\bullet}; \overline{\mathcal{C}}_{\bullet}$	Centile or percentile of \bullet ; its discrete Monte Carlo approximation
CL	Confidence level
$CI^{\bullet}; CI_{left}^{\bullet}$	Confidence interval for the discrete stochastic quantity \bullet ; its left sub-interval w.r.t. the median
$\{Z_{jZ}\}_{jZ=1}^{jZ=n_Z}$	Polynomial basis in a Polynomial Chaos Expansion (PCE)
$\sigma; n_Z$	Maximum order in the PCE determining its n_Z number of polynomials (with r and truncation)
$\mathbf{w}^{\mathfrak{h}}; \widehat{\mathbf{w}}$	Weights for the PCE approximation of the model in the spaces $\mathcal{V}^{\mathfrak{h}}$ and $\widehat{\mathcal{V}}$ (same basis)
CP; \bullet^{CP}	Control points; quantity \bullet computed through CP
\bullet_{PC^o}	Quantity \bullet approximated with PCE surrogate model of maximum polynomial order σ
$\{\mathcal{Q}_{b*}^{\mathfrak{h}}\}_{b*=1}^{b*=n_b}$	Family of n_{b*} sets of bootstrapped outcomes of $Q^{\mathfrak{h}}$ used to estimate its variance

3 Reference parametrised problem and notation

3.1 Parametrised frequency-domain structural vibration problem

This section introduces the class of parametrised elasticity problems that we are interested in. We consider the undamped, steady-state vibrations of a structure occupying a bounded domain $\Omega \subset \mathbb{R}^d$, with $d = 2$ or $d = 3$. We assume that the equations of isotropic linear elasticity govern the deformation of the structure, and small deformations are assumed. The Young's modulus is a function of space and

is parametrised by means of a finite set of real-valued variables. Therefore, so it is the Hook tensor.

Within this framework, the differential equation describing the conservation of linear momentum reads

$$\begin{aligned} \left(\rho \frac{\partial^2}{\partial t^2} - \nabla_s \cdot (C(\mathbf{x}, \boldsymbol{\mu}) \nabla_s) \right) U(\mathbf{x}, \boldsymbol{\mu}, t) &= F(\mathbf{x}, t) \quad \text{in } \Omega, \\ U(\mathbf{x}, \boldsymbol{\mu}, t) &= U_d(\mathbf{x}, t) \quad \text{on } \Gamma_d, \\ (C(\mathbf{x}, \boldsymbol{\mu}) \nabla_s U(\mathbf{x}, \boldsymbol{\mu}, t)) \cdot \vec{n} &= G_n(\mathbf{x}, t) \quad \text{on } \Gamma_n. \end{aligned} \quad (1)$$

In the previous equations, Γ_n and Γ_d stand for the complementary subsets of the boundary $\partial\Omega$ where Neumann and Dirichlet conditions are prescribed, respectively, and defined such that Γ_d is neither empty nor reduced to points. In particular, $U_d(\mathbf{x}, t) : \Gamma_d \times \mathcal{T} \rightarrow \mathbb{R}^d$ stands for the prescribed boundary displacement and $G_n(\mathbf{x}, t) : \Gamma_n \times \mathcal{T} \rightarrow \mathbb{R}^d$ for the prescribed boundary traction, where the bounded time interval is denoted as \mathcal{T} . The given vector-valued $F(\mathbf{x}, t) : \Omega \times \mathcal{T} \rightarrow \mathbb{R}^d$ is a forcing function depending on time and space. The parametric uncertainty in the Young's modulus field $E(\mathbf{x}, \boldsymbol{\mu})$ is accounted by a r -dimensional primary variable $\boldsymbol{\mu} \in \Theta \subset \mathbb{R}^r$ in the form of a vector of real parameters. The fourth order Hooke tensor $C(\mathbf{x}, \boldsymbol{\mu}) \equiv C(E(\mathbf{x}, \boldsymbol{\mu}), \nu)$ describes isotopic linear elasticity, being ν is the deterministic Poisson's ratio. Mass density is assumed to be constant and it is denoted by ρ . Finally, the vector-valued field of displacements $U(\mathbf{x}, t, \boldsymbol{\mu}) : \Omega \times \Theta \times \mathcal{T} \rightarrow \mathbb{R}^d$ depends on time and the random parameters described by $\boldsymbol{\mu}$.

Frequency-domain solutions to (1) are chosen as representative numerical problem to solve. It is relevant enough to raise the interaction between discretisation and probabilistic errors. Although less accurate than time-domain analysis (for which the algorithm can also be applied), there exist a vast number of applications where these non-hyperbolic solutions are useful (*e.g.* to predict cracks in structures [37]). Assuming that the loading functions are time-harmonic, *i.e.* $F(\mathbf{x}, t) = f(\mathbf{x}; \omega) e^{i\omega t}$, $U_d(\mathbf{x}, t) = u_d(\mathbf{x}; \omega) e^{i\omega t}$, $G_n(\mathbf{x}, t) = g_n(\mathbf{x}; \omega) e^{i\omega t}$, we look for steady-state waves of the form $U(\mathbf{x}, t, \boldsymbol{\mu}) = u(\mathbf{x}, \boldsymbol{\mu}; \omega) e^{i\omega t}$. Where the symbol $i = \sqrt{-1}$ is used, and ω is the angular frequency associated with the harmonic loading function. The structural dynamic system equation in the frequency domain of a given ω is then:

$$\begin{aligned} - \left(\rho \omega^2 + \nabla_s \cdot (C(\mathbf{x}, \boldsymbol{\mu}) \nabla_s) \right) u(\mathbf{x}, \boldsymbol{\mu}) &= f(\mathbf{x}) \quad \text{in } \Omega, \\ u(\mathbf{x}, \boldsymbol{\mu}) &= u_d(\mathbf{x}) \quad \text{on } \Gamma_d, \\ (C(\mathbf{x}, \boldsymbol{\mu}) \nabla_s u(\mathbf{x}, \boldsymbol{\mu})) \cdot \vec{n} &= g_n(\mathbf{x}) \quad \text{on } \Gamma_n. \end{aligned} \quad (2)$$

Let \mathcal{V} and \mathcal{U} be the test and trial Sobolev spaces $\mathcal{V} = \{v \in \mathcal{H}^1(\Omega) \mid v = 0 \text{ on } \Gamma_d\}$ and $\mathcal{U} = \{u \in \mathcal{H}^1(\Omega) \mid u = u_d \text{ on } \Gamma_d\}$. Then, the variational form of the equation (2) becomes, find $u \in \mathcal{U}$ such that

$$\begin{aligned} \int_{\Omega} \left(\rho \omega^2 v(\mathbf{x}) \cdot u(\mathbf{x}, \boldsymbol{\mu}) + \nabla v(\mathbf{x}) \cdot (C(\mathbf{x}, \boldsymbol{\mu}) \nabla_s u(\mathbf{x}, \boldsymbol{\mu})) \right) d\Omega \\ = \int_{\Omega} v(\mathbf{x}) \cdot f(\mathbf{x}) d\Omega + \int_{\Gamma_n} v(\mathbf{x}) \cdot g_n(\mathbf{x}) d\Gamma_n \quad \forall v(\mathbf{x}) \in \mathcal{V}. \end{aligned} \quad (3)$$

For the sake of simplicity, notations $a^\omega(\cdot, \cdot; \cdot)$ and $l(\cdot)$ are introduced to match both sides of equation (3), which now simply reads as

$$a^\omega(u, v; \boldsymbol{\mu}) = l(v), \quad \forall v \in \mathcal{V}. \quad (4)$$

3.2 Parametrised problem of interest

In order to guide the reader, we give a visual example of the type of structural vibration problem that we are interested in. The mechanical problem under consideration is represented in figure 1, where the geometry, load case and tunable/unknown parameters are all represented graphically.

P1, P2 and P3 are different loading cases, being the load $f(\mathbf{x})$ uniformly distributed and of unitary value in the direction of the arrows. Load P1 (that is applied in direction $-\vec{e}_{x_1} = (-1, 0)$ to $\{\mathbf{x} \in \mathbb{R}^2 : x = L, y = [L + 0.5, 2L]\}$) excites the 1st natural frequency of the structure, load P2 (in direction

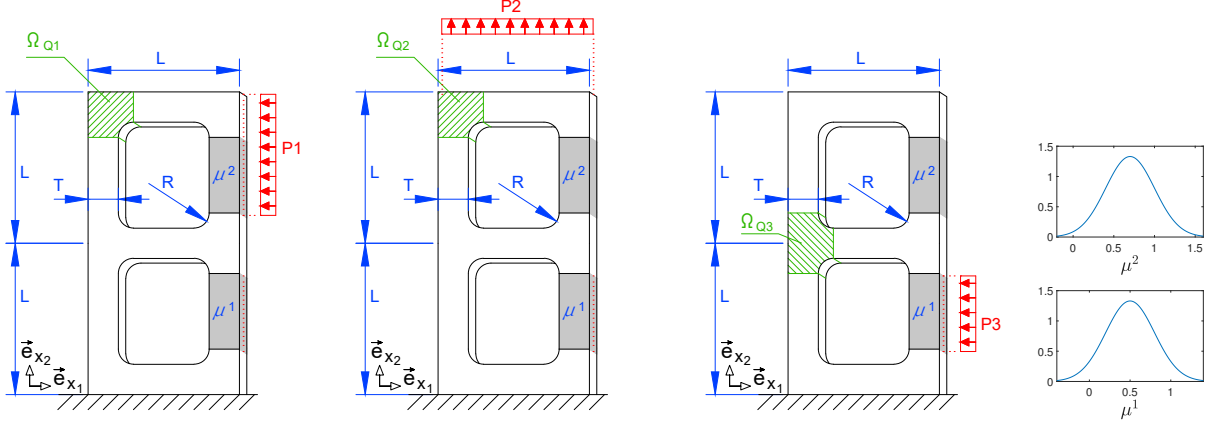


Figure 1: Geometry parameters for the numerical examples

$\vec{e}_{x_2} = (0, 1)$ applied to $\{\mathbf{x} \in \mathbb{R}^2 : x = [0, L], y = 2L\}$ produces horizontal displacement only due to the parametric uncertainty and load P3 (in direction $\vec{e}_{x_1} = (-1, 0)$ applied to $\{\mathbf{x} \in \mathbb{R}^2 : x = L, y = [T + R, L - 0.5T - R]\}$) is included only to test the indicator of refinement, which should concentrate in the lower half of the structure.

Formally, we introduce the domain of the structure as

$$\Omega = \{[0, L] \times [0, 2L]\} \setminus \{\Omega_{H1} \cup \Omega_{H2}\}, \quad (5)$$

where

$$\begin{aligned} \Omega_{H1} = & \{\mathbf{x} \in \mathbb{R}^2 : |\mathbf{x} + (T + R, T + R)| < R\} \cup \\ & \{\mathbf{x} \in \mathbb{R}^2 : |\mathbf{x} + (L - T - R, T + R)| < R\} \cup \\ & \{\mathbf{x} \in \mathbb{R}^2 : |\mathbf{x} + (T + R, L - 0.5T - R)| < R\} \cup \\ & \{\mathbf{x} \in \mathbb{R}^2 : |\mathbf{x} + (L - T - R, L - 0.5T - R)| < R\} \cup \\ & \{[T + R, L - T - R] \times]T, L - 0.5T[\} \cup \\ & \{[T, L - T[\times]T + R, L - 0.5T - R]\}, \end{aligned} \quad (6)$$

the symbol (\cdot, \cdot) denotes a vector in \mathbb{R}^2 , symbols $[\cdot, \cdot]$ and $]\cdot, \cdot[$ are closed and open intervals in \mathbb{R} , and

$$\Omega_{H2} = \{\mathbf{x} \in \mathbb{R}^2 : \mathbf{x} - (0, L - 0.5T) \in \Omega_{H1}\}. \quad (7)$$

Furthermore, Ω is divided in a non-overlapping domain decomposition $\Omega = \bigcup_{i=0}^r \Omega_i$ with $r = 2$ number of parametric dimensions and $(\Omega_i - \partial\Omega_i) \cap (\Omega_j - \partial\Omega_j) = \{\emptyset\}$ if $i \neq j$. We then establish the following expression for the Hooke tensor field $C(\mathbf{x}, \boldsymbol{\mu})$:

$$C(\mathbf{x}, \boldsymbol{\mu}) \nabla_s(\cdot) = \frac{e^{\mu^i} \nu}{(1 + \nu)(1 - 2\nu)} \text{Tr}(\nabla_s(\cdot)) \mathbb{I} + \frac{e^{\mu^i}}{(1 + \nu)} \nabla_s(\cdot) \quad \text{if } \mathbf{x} \in \Omega_i, i \geq 1, \quad (8)$$

where \mathbb{I} is an identity fourth order tensor of appropriate dimension.

In the non-parametric domain $\Omega_0 = \Omega \setminus \{\Omega_1 \cup \Omega_2\}$, we set the Young's modulus 1, which is the reference value. In the parametric subdomains $\Omega_{i \neq 0}$, the Young's modulus is defined by means of known primary statistical variables (For instance precast concrete is used and the factory provides this data). In our specific case these parametric subdomains are located in $\Omega_1 = [L - T, L] \times [T + R, L - 0.5T - R]$ and $\Omega_2 = [L - T, L] \times [L + 0.5T + R, 2L - T - R]$, and the probabilistic description is provided in section 6. These parametric variables produce an unknown dependent variable or response surface.

Regarding the probabilistic model for the Young's modulus, Steel C. [38] proposes a normal distribution justified by the central limit theorem applied to homogenisation and verifies it experimentally. Yet, since the present work does not correspond to any experimental data, in order to ensure that any C remains strictly positive regardless of the outcome of $\boldsymbol{\mu}$, its i^{th} component μ^i (associated with

the darkened domains Ω_i) represents the logarithm of the local Young's modulus. The results presented in the present work are produced with known probabilistic primary parameters consisting on a uncorrelated normal distribution. The exact values are defined at section 6.

As main example of QoI, we will measure the displacement in direction $\vec{e}_x \in \mathbb{R}^d$ averaged over a sub-domains Ω_\bullet . Namely,

$$q(u(\mathbf{x}, \boldsymbol{\mu})) := \frac{1}{|\Omega_{Q_\bullet}|} \int_{\Omega_{Q_\bullet}} \vec{e}_x \cdot u(\mathbf{x}, \boldsymbol{\mu}) dx, \quad (9)$$

where Ω_\bullet varies depending on the loading case, being $\Omega_{Q1} = \Omega_{Q2} := \Omega \setminus \{[0, T+R] \times [2L-T-R, 2L]\}$ and $\Omega_{Q3} := \Omega \setminus \{[0, T+R] \times [L-0.5T-R, L+0.5T+R]\}$ where the numerical indexes refer to P1, P2 and P3.

Strains will be used as alternative QoI to check independence of results with respect the former QoI. Furthermore, subdomain mesh constrains will be overcome by substituting subdomain integration by a normal distributed weight with mean centered in the area of interest. The weighted XY strain component concentrated in the top right corner reads

$$q(u(\mathbf{x}, \boldsymbol{\mu})) := \mathcal{N}([T; 2L-T], [L, 0; 0, L]) 0.5 \int_{\Omega} \frac{\partial}{\partial y} \vec{e}_x \cdot u(\mathbf{x}, \boldsymbol{\mu}) + \frac{\partial}{\partial x} \vec{e}_y \cdot u(\mathbf{x}, \boldsymbol{\mu}) d\Omega. \quad (10)$$

Both resultant random variables $q(u(\mathbf{x}, \boldsymbol{\mu}))$ depend on the forwarded uncertainty propagation of the primary variables $\boldsymbol{\mu}$ and the errors on their discrete evaluation depend also on the level of discretisation ($u^h(\mathbf{x})$ corresponding to a given mesh). Their characterisation requires multiple evaluations of the FE model in order to approximate probabilistic measures (details in section 4). Furthermore, its accuracy depends on the discretisation while its reliability on the number of evaluations. This paper proposes an algorithm to achieve a precise and trustful characterisation with minimal computational cost. The algorithm presented could be used to compute any probabilistic measure of the QoI, but their expectation and percentiles are selected in the present work.

3.3 Goal-oriented error estimation

The discrete local estimation of the defined QoI driving the greedy-based refinement process will be presented in this section.

Historically, so-called “energy-norm” error indicators were used to guide the refinement strategy. They include finite element post-processing methodologies such as those based on the constitutive relation error [39, 40], gradient recovery [41] and residual estimators [42, 43]). Nowadays, and thanks to the pioneering work of Becker and Rannacher [44], Cirak and Ramm [45] and Oden and Prudhomme [46] in particular, goal-oriented a posteriori methods allow us to guide refinement process so that the precision of the actual QoI of the finite element problem is (sub-)optimised. These techniques are well-understood in the context of linear and mildly non-linear diffusive problems.

FEM will be used to seek approximate solutions to the vibration problem. To this end, the exact variational formulation is replaced by its discretised counterpart

$$a^\omega(u^h, v^h; \boldsymbol{\mu}) = l(v^h), \quad \forall v^h \in \mathcal{V}^h. \quad (11)$$

Coarse spaces $\mathcal{V}^h \subset \mathcal{V}$ and $\mathcal{U}^h \subset \mathcal{U}$ are defined through a mesh \mathcal{M}_m of non-overlapping linear (p1) triangular elements forming the approximative tessellated domain $\Omega_h \subset \Omega$. The solution and test FE fields are then piecewise linear, and we will neglect the influence of the geometrical error. Subsequently, we will drop notation Ω_h and abusively denote $\Omega \equiv \Omega_h$ indistinctly for discrete polygonal and whole non-polygonal domains.

The discretisation error $e(\mathbf{x}, \boldsymbol{\mu}) = u(\mathbf{x}, \boldsymbol{\mu}) - u^h(\mathbf{x}, \boldsymbol{\mu})$ belongs to the space \mathcal{V} of homogeneous fields since both $u(\mathbf{x}, \boldsymbol{\mu})$ and $u^h(\mathbf{x}, \boldsymbol{\mu})$ are exact at Γ_d in the presented case. Furthermore, it is the solution of the following boundary value problem

$$a^\omega(e, v; \boldsymbol{\mu}) = l(v) - a^\omega(u^h, v; \boldsymbol{\mu}), \quad \forall v \in \mathcal{V}. \quad (12)$$

We define the residual form over \mathcal{V} as

$$\mathcal{R}^\omega(v; \boldsymbol{\mu}) := l(v) - a^\omega(u^h, v; \boldsymbol{\mu}). \quad (13)$$

We choose to approximate the error $e(\mathbf{x}, \boldsymbol{\mu})$ through the definition of a discrete rich space $\widehat{\mathcal{V}} \subset \mathcal{V}$ consisting in the same mesh \mathcal{M}_{m} with quadratic triangles and the edge nodes exactly at the midpoint of the edges. The reason is that even if the re-entrant corners create singularities, vibration problem solutions are smooth, and therefore a more accurate global solution is ensured. The adaptive refinement strategy is based on the size of the element, so h-refinement (reduction of the element size) will take into the account the singularities that the p-refinement (increase of the order of the polynomial shape function) can capture even if less efficiently. Consequently, the solution \widehat{u} is computed and considered close enough to u for the sole purpose of driving each refinement iteration. This leads to the approximation

$$e(\mathbf{x}, \boldsymbol{\mu}) = u(\mathbf{x}, \boldsymbol{\mu}) - u^{\text{h}}(\mathbf{x}, \boldsymbol{\mu}) \approx \widehat{e}(\mathbf{x}, \boldsymbol{\mu}) := \widehat{u}(\mathbf{x}, \boldsymbol{\mu}) - u^{\text{h}}(\mathbf{x}, \boldsymbol{\mu}), \quad (14)$$

which is computable directly through FEM and interpolation without any other error estimation technique. Of course, any error estimator could be used instead and similar results are to be expected with the only exception of problems with highly non-smooth solutions in the interior domain.

The error in the QoI is defined using equation 9 and assuming linearity as

$$\epsilon^Q(\boldsymbol{\mu}) := q(u(\mathbf{x}, \boldsymbol{\mu})) - q(u^{\text{h}}(\mathbf{x}, \boldsymbol{\mu})) = q(e(\mathbf{x}, \boldsymbol{\mu})). \quad (15)$$

A sample evaluation of this QoI is a scalar representing a global magnitude. In order to obtain a dual of $q(e(\mathbf{x}, \boldsymbol{\mu}))$ defined in all the domain, the adjoint problem [46] is introduced. It contains all Residual information (as any error estimator or indicator based on it) and reads

$$a^\omega(v(\mathbf{x}, \boldsymbol{\mu}), z(\mathbf{x}, \boldsymbol{\mu})) := q(v(\mathbf{x}, \boldsymbol{\mu})) = \mathcal{R}^\omega(z; \boldsymbol{\mu}), \quad \forall v(\mathbf{x}, \boldsymbol{\mu}) \in \mathcal{V}. \quad (16)$$

Using the definition 13 we obtain the dual-weighted form

$$\mathcal{R}^\omega(e; \boldsymbol{\mu}) = q(e(\mathbf{x}, \boldsymbol{\mu})) = a^\omega(e(\mathbf{x}, \boldsymbol{\mu}), z(\mathbf{x}, \boldsymbol{\mu})). \quad (17)$$

The *influence field* or *influence function* denoted as field $z(\mathbf{x}, \boldsymbol{\mu})$ reflects the residual influence upon the QoI. Equation 16 allows to compute discrete approximations of this field. Most importantly, local indicators of $z(\mathbf{x}, \boldsymbol{\mu})$ can be obtained by applying any partition of unity ϕ_i

$$\mathcal{R}^\omega(z; \boldsymbol{\mu}) = \sum_i \mathcal{R}^\omega(\phi_i z; \boldsymbol{\mu}). \quad (18)$$

4 Forward Uncertainty Propagation

4.1 Stochastic computational model and Monte Carlo method

In the previous sections, we have defined a deterministic computational model \mathfrak{M} that given a sample of the primal parameter variable $\boldsymbol{\mu}$ produces an outcome for any QoI which is a dependent variable. This section poses the functional stochastic problem to solve (mapping from $\boldsymbol{\mu}$ to the response surface) where the function is the numerical model which also depends on the spatial mesh used to discretise the problem. The expectation and percentiles of the QoI(s) were selected as measures to characterise the response surface(s).

MC methods [47, 48, 49] constitute the simplest option but several alternatives exist that reduce the amount of sampling required to characterise stochastic processes (*i.e.* collocation [50, 10], adaptive sampling [9], sparse grid sampling [51] or importance sampling [52]). Although the paper focusses on forward uncertainty propagation, the present work could be extended to inverse uncertainty characterisation based on MC or Markov Chain MC [53] sampling techniques (*e.g.* [54, 55, 56]).

Let us define the stochastic problem in the following probabilistic space. Firstly, the sampling space is $\Theta \subset \mathbb{R}^r$. Secondly the Borel σ -algebra consists of the collection \mathcal{F} of all measurable subsets \mathcal{S}_{i_S} of Θ including the empty subset. The collection \mathcal{F} is closed under complements and also under countable unions. Finally, the probability that the outcome of $\boldsymbol{\mu}$ is included in a measurable subset of \mathcal{F} reads $\mathcal{P}(\boldsymbol{\mu} \in \mathcal{S}_{i_S}) = \int_{\mathcal{S}_{i_S}} f_{\boldsymbol{\mu}}^{\mathcal{P}}(\boldsymbol{\mu}) d\boldsymbol{\mu}$, where the probability density function (PDF) $f_{\boldsymbol{\mu}}^{\mathcal{P}}$ is known.

Each given mesh \mathcal{M}_m processed by the numerical model $\mathfrak{M}(\boldsymbol{\mu})$ produces an unknown stochastic process for the QoI response due to the forward uncertainty propagation of the primary random parameters. The PDF f_Q^p defining the response random variable $Q_m : \Theta_Q \mapsto \mathbb{R}$ is unknown. Nevertheless, it is a dependent variable, function of the independent parametric variable; *i.e.* $Q_m(\theta_Q) \equiv Q_m(\boldsymbol{\mu}, \mathcal{M}_m)$. Therefore, exploiting the surjective non-injective map existing between both sampling spaces leads to

$$\mathfrak{M}(\boldsymbol{\mu}) : \Theta \mapsto Q_m, \quad (19)$$

where $\boldsymbol{\mu} \in \Theta \subseteq \mathbb{R}^r$ and $Q_m = q(u(\boldsymbol{\mu}(\boldsymbol{\theta}))) \in \Theta_Q \subseteq \mathbb{R}$. That is to say, the numerical FEM model maps $\boldsymbol{\mu} \in \mathbb{R}^r$ to $Q_m \in \mathbb{R}$, both being random variables.

Monte-Carlo integration will allow us to evaluate numerically some statistical measures of the dependent variable. It is important to note that to evaluate the statistical QoI, we will keep our computational mesh fixed. The subindex referring to a specific mesh will be dropped henceforth unless necessary.

Any statistical measure or collection of them can be selected as a solution for the stochastic problem. In this work, we are particularly interested in the expectation of the QoI. However, since the selected surrogate model can produce an expectation directly, we will look also to percentiles.

Recalling the definition of the expectation of a response random variable Q

$$\mathcal{E}[Q] \equiv \mathcal{E}[\mathfrak{M}(\boldsymbol{\mu})] := \int_{\Theta} Q f_{\boldsymbol{\mu}}(\boldsymbol{\mu}) d\boldsymbol{\mu}. \quad (20)$$

Around any measure it is also needed to assess the uncertainty. Confidence intervals [57] and confidence levels using percentiles are the most extended option and so the one used. Quantiles, statistical moments or analysis of the full distribution are alternative valid assessments.

Since the PDF of $\boldsymbol{\mu}$ is known, MC sampling allows to approximate the PDF f_Q^p by evaluating ns samples $Q_s = \mathfrak{M}(\boldsymbol{\mu}_s)$ ruled by the known distribution $f_{\boldsymbol{\mu}}^p(\boldsymbol{\mu})$. Mathematically,

$$\mathcal{E}[Q] \approx \overline{\mathcal{E}}[Q] := \frac{1}{ns} \cdot \sum_{s=1}^{ns} \mathfrak{M}(\boldsymbol{\mu}_s) = \frac{1}{ns} \cdot \sum_{s=1}^{ns} Q_s, \quad \boldsymbol{\mu}_s \sim f_{\boldsymbol{\mu}}(\boldsymbol{\mu}). \quad (21)$$

The percentiles are computed by the closest rank method with linear interpolation, using the set of evaluated samples. We will keep the distinct notation C_i and \overline{C}_i for analytical and discrete (*i.e.* computed from available samples) for the i -th percentile respectively.

These evaluations involve computing the whole FE problem whose computational cost is high. Moreover, the convergence rate of MC sampling methods is \sqrt{ns} even assuming perfect random number generation. This means that each additional order of magnitude precision requires to square the sample size.

4.2 Surrogate model

In order to reduce the cost of the evaluations of the full numerical model, a surrogate model will be built. The surrogates can be based on functional expansion [14, 15] or numerical integration [58, 59]. This work will employ standard Polynomial Chaos Expansion (Wiener Chaos or PCE) with tensor product of 1D Hermite polynomials, which makes the construction of the multidimensional surrogate straightforward. Conversely, numerical integration based methods build the surrogate after the computation of some moments. Another benefit of PCE surrogates is that their accuracy is adaptively adjustable and only dependent on the maximum order of polynomials used in the expansion, which perfectly fits the adaptive algorithm presented. Regarding accuracy, the work by Lee and Cheng [60] shows that they can be as accurate as any other method provided that enough order of polynomials are considered in the expansion. In order to avoid the introduction of more local error phenomena, only standard PCE is implemented with no local enrichment of the surrogate.

Remark. *Even though PCE can be fitted to represent the probability response surface directly allowing also to compute surrogate model expectation analytically (not the percentiles), in the present work it is only used as a reduced model in order to minimise the offline computational time. The*

algorithm presented in this work is independent of the model. Therefore, no surrogate model or any other reduced model could be used, even if it is not able to represent the random dependent variable. Its only requirement is being able to produce outcomes of the dependent variable from a sample of the set of primary variables.

4.3 Total error and error contributions

After the definition of all building-blocks of the problem posed and the chain of approximations, the total error in QoI's expectation or i^{th} percentile can be expressed as

$$\epsilon := \mathcal{E}[Q] - \overline{\mathcal{E}}[Q_{PC}^h] \quad \text{for the expectation,} \quad (22a)$$

$$\epsilon := C_i[Q] - \overline{C}_i[Q_{PC}^h] \quad \text{for } i\text{-th percentiles.} \quad (22b)$$

Here, the different approximations are denoted by (1) superindex h standing for the spatial discretisation belonging to the coarse space \mathcal{V}^h , (2) subindex PC indicating the surrogate approximation due to PCE, and (3) the operators $\overline{\mathcal{E}}[\cdot]$, $\overline{C}_i[\cdot]$ (see equation 21 and next paragraph) including the finite sampling approximation resulting from MC method.

Henceforth, the symbol $\hat{\cdot}$ introduced in equation 14 will be extended to all magnitudes belonging to the spaces $\hat{\mathcal{V}}$ or $\hat{\mathcal{U}}$, which are always the quadratic enrichment space of the linear element defined spaces $\mathcal{V}^h \subset \hat{\mathcal{V}} \subset \mathcal{V}$ or $\mathcal{U}^h \subset \hat{\mathcal{U}} \subset \mathcal{U}$ respectively. For the sake of simplicity we introduce the notation p1 for spaces defined by linear elements and p2 for quadratic elements.

The errors associated with the aforementioned approximation of the expectation can be expressed as

$$\epsilon = \underbrace{(\mathcal{E}[Q] - \mathcal{E}[\hat{Q}])}_{\tilde{\epsilon}} + \underbrace{(\mathcal{E}[\hat{Q}] - \overline{\mathcal{E}}[\hat{Q}])}_{\bar{\epsilon}} + \underbrace{(\overline{\mathcal{E}}[\hat{Q}] - \overline{\mathcal{E}}[\hat{Q}_{PC}])}_{\epsilon_{PC}} + \underbrace{(\overline{\mathcal{E}}[\hat{Q}_{PC}] - \overline{\mathcal{E}}[Q_{PC}^h])}_{\hat{\epsilon}}, \quad (23)$$

ϵ_{NM}

where $\bar{\epsilon}$ corresponds to MC error (*i.e.* statistical sampling error), ϵ_{PC} to surrogate or PCE error, and both $\hat{\epsilon}$ and $\tilde{\epsilon}$ to discretisation error. The non-computable part of the discretisation error $\tilde{\epsilon}$ can be easily checked by means of standard convergence analysis or error estimators with guaranteed lower and upper bounds such as flux-free locally equilibrated error estimates [61]. Due to the fact that in the vibration problems we are interested in, both the spatial solution field u and the stochastic field remain smooth with the only exception of the parameters leading exactly to a natural frequency, the present work will use an error estimation based on projection of polynomial order easier to implement but not reliable on non-smooth cases. For completeness, section 6.2 includes a standard convergence check with respect to a reference solution (see figure 14).

Lastly, the *numerical approximation error* is defined as ϵ_{NM} . Its PCE part is fully controlled through pre-calibration of the PCE at each mesh refinement step. Afterwards, ϵ_{PC} and $\hat{\epsilon}$ cannot be assessed separately, unless unwanted further evaluations of the FE model are computed (see section 5.1 for details).

An equivalent expression to equation 23 and to all derived subsequent equations for percentiles can be obtained from 22.b. For the sake of concision, henceforth equivalent equations referring to percentiles will be omitted in the paper unless required.

5 Simultaneous evaluation and control of Monte-Carlo, surrogate model and Finite Element numerical errors

The algorithm presented aims to deliver an optimised computational mesh, with minimum computational effort while satisfying a given accuracy dictated by either the expectation or the percentile of the engineering QoI. The refinement algorithm is iterative, and henceforth, we describe the numerical operations that will be performed at iteration i of this algorithm. Several important steps need to be described in detail: (i) how to control the quality of the PCE, (ii) how to compare the statistical error $\bar{\epsilon}$ and the numerical approximation error ϵ_{NM} (surrogate model + FEM discretisation) and subsequently decide which of the two needs to be reduced and (iii) how to perform local mesh adaptivity in this setting.

5.1 Adaptive surrogate model strategy

As a step towards a full adaptive uncertainty propagation algorithm, this subsection explains how to jointly control FE discretisation and PCE errors.

The maximum order σ of the polynomial considered in the basis \mathcal{Z} determines both the precision of PCE and the number of Hermite-Gauss quadrature points to evaluate through the model \mathfrak{M} . A perfect surrogate model would produce exactly the same outcome than the full FE model. Therefore, the required PCE precision depends on the discretisation error. Consequently, PCE error can be neglected in ϵ_{NM} provided it is at least one order of magnitude smaller than discretisation error.

5.1.1 Measures of the discretisation error extended to the parameter space

The chosen surrogate model's error is defined in the parameter space whereas the discretisation error is defined for a single sampling point. Therefore, in order to compare them and enforce the desired balance, the latter must be extended to the parameter space.

Discretisation error $\widehat{\epsilon}_{m_s} := |\widehat{Q}_{m_s} - Q_{m_s}^h|$ is deterministic given a mesh \mathcal{M}_m and a sampling point s . Exact values of this error are only computed at the quadrature points as shown in figure 10 and 11.

In order to control PCE surrogate this error must be extended to Θ , for instance considering:

$$\text{The maximum in } \Theta, \quad \widehat{\epsilon}_m^\Theta = \max_{\Theta} |\widehat{Q}_{m_s} - Q_{m_s}^h|, \quad (24a)$$

$$\text{Stat. moment order } \tilde{o}, \quad \widehat{\epsilon}_m^\Theta = \int_{\Theta} |\widehat{Q}_{m_s} - Q_{m_s}^h|^{\tilde{o}} f_{\boldsymbol{\mu}}(\boldsymbol{\mu}) d\boldsymbol{\mu}, \quad (24b)$$

$$\text{The average in } \Theta, \quad \widehat{\epsilon}_m^\Theta = \frac{1}{ns} \sum_{s=1}^{ns} |\widehat{Q}_{m_s} - Q_{m_s}^h|, \quad (24c)$$

where ns denotes the number of evaluated samples s .

The present work discards the maximum criterion because of it highly depends on the set of samples used as control points to fit the surrogate model. As can be seen in figure 11, PCE accuracy worsens as the distance from a given sample to the area of maximum probability increases. Then, the average (equation 24c, even if it is not a norm) was selected for two reasons. First, the expectation of the QoI was selected as one of the measures of the stochastic problem in section 4.1 and it follows the same principle as how MC estimates the expectation (see equation 21). Second, all studied stochastic measures (expectation and percentiles) are order one, so it seems unnecessary to use moments of higher order.

5.1.2 Calibration of the surrogate model

Sampling for the calibration. For a fixed maximum order σ considered in PCE reduced model, the assessment of PCE precision requires two different sets of sampling points to be evaluated with the FE model. The first set is fixed and corresponds to the Gauss-Hermite quadrature points evaluated in the least squares fitting process. The second one serves the purpose of computing measure 24c.

We introduce the denomination *control points* for the second set in order to separate it from the MC set of samples. Two things must be considered to size this set, the variance in the estimation of the fitting measure (especially in the case of small σ polynomials) and the cost needed to compute it. Since the first criterion is more important, a user defined minimum was implemented to guarantee contributions from all relevant sectors of the domain and avoid an undue high variance. In the present work the chosen minimum number of control samples is 400. From that number, we propose to pair the number of quadrature and control points. This way, the evaluation cost of the fitting and the assessment processes increase proportionally, which does not hamper the global cost.

Subalgorithm 1 is devised to minimise the number of evaluations needed. Incremental σ are tried until the measure 24c is smaller than a 10 %, ensuring PCE error is negligible with respect to the discretisation error. Since refining the mesh results generally in a more complex response surface, σ is saved to re-initialise the subalgorithm after mesh refinement.

Calibration sub-algorithm. From equation 24c and using index s' to denote the n_{CP} control sampling points $\theta_{s'} \in \Theta$, the measure $\widehat{\epsilon}_m^{CP}$ reads

$$\widehat{\epsilon}_m^{CP} = \frac{1}{n_{CP}} \sum_{s'=1}^{n_{CP}} |\widehat{Q}_{ms'} - Q_{ms'}^h|, \quad \text{where } \theta_{s'} \neq \theta_s, \quad \forall s' \in S' = \{1, \dots, n_{CP}\}, \quad (25)$$

$$\forall s \in S = \{1, \dots, ns\},$$

where the index s denotes the ns MC sampling points $\theta_s \in \Theta$.

To compute the PCE approximation of measure $\widehat{\epsilon}_m^{CP}$, two different surrogate models are fit for each mesh \mathcal{M}_m , corresponding to the coarse p1 and fine p2 spaces. Then,

$$\widehat{Q}_{ms', PC^o} = \sum_{j_Z=1}^{j_Z=n_Z} \widehat{w}_{j_Z} Z_{j_Z}(\theta_{s'}), \quad 1^{st} \text{ PCE for } \widehat{Q}_m, \quad (26a)$$

$$Q_{ms', PC^o}^h = \sum_{j_Z=1}^{j_Z=n_Z} w_{j_Z}^h Z_{j_Z}(\theta_{s'}), \quad 2^{nd} \text{ PCE for } Q_m^h, \quad (26b)$$

$$\widehat{\epsilon}_{mPC^o}^{CP} = \frac{1}{n_{CP}} \sum_{s'=1}^{n_{CP}} |\widehat{Q}_{ms', PC^o} - Q_{ms', PC^o}^h| \quad \text{approximated measure}, \quad (26c)$$

where the two different weighting coefficient sets $\widehat{\mathbf{w}} = \{\widehat{w}_{j_Z}\}_{j_Z=1}^{j_Z=n_Z}$ and $\mathbf{w}^h = \{w_{j_Z}^h\}_{j_Z=1}^{j_Z=n_Z}$ for the same basis $\{Z_{j_Z}\}_{j_Z=1}^{j_Z=n_Z}$ fixed by o are fitted through least squares thanks to the orthogonality between basis components (distinct tensor products of 1D Hermite polynomials) weighted by the target Gaussian distribution.

The difference between these two PCE approximations is the response surface shown in figure 10. And the measure defined in 26.c is the MC integration of this surface. In this work, calibration consists in ensuring that the response surface for the error in the QoI is of the same order than the one that should have been produced sampling intensively the original FE model. Graphically, the error in this response surface is the vertical distance between the surface and the exact values at the quadrature points (figures 10 and 11).

Set a minimum of Control Points (min_{CP}) to ensure low variance

```

while  $|\widehat{\epsilon}_{mPC^o}^{CP} - \widehat{\epsilon}_m^{CP}|/|\widehat{\epsilon}_m^{CP}| > 10\%$  and  $1/n_{CP} \sum_{s'=1}^{n_{CP}} (|\widehat{Q}_{ms', PC^o} - Q_{ms'}^h|/|\widehat{Q}_{ms'}|) > 10\%$  do
    Increase order  $o$  of the maximum polynomial and number of quadrature points ( $n_{QP}$ )
    Check if the number of Control Points needs to be increased (if  $n_{QP} > min_{CP}$ , then  $n_{CP} = n_{QP}$ )
    Compute solution at new quadrature and control points
    Update  $\widehat{\epsilon}_m^{CP}$  with new samples
    Least squares to update the coefficients of polynomial chaos
    Compute approximation at control points and  $\widehat{\epsilon}_{mPC^o}^{CP}$ 
end

```

Subalgorithm 1: Calibration of polynomial chaos surrogate(s) for mesh \mathcal{M}_m

In order to avoid a case where the reduced order of magnitude of discretisation error using PCE comes from compensation of PCE errors, an extra condition is needed. Then the two conditions to ensure both PCE approximations are correctly calibrated read

$$|\widehat{\epsilon}_{mPC^o}^{CP} - \widehat{\epsilon}_m^{CP}|/|\widehat{\epsilon}_m^{CP}| < 10\%, \quad (27a)$$

$$\frac{1}{n_{CP}} \sum_{s'=1}^{n_{CP}} (|\widehat{Q}_{ms', PC^o} - Q_{ms'}^h|/|\widehat{Q}_{ms'}|) < 10\%. \quad (27b)$$

After calibration, both surrogate models produce outcomes of \widehat{Q}_{ms', PC^o} and Q_{ms', PC^o}^h with negligible PCE component. That is to say $\epsilon_{PC} \ll \widehat{\epsilon}$. Therefore, for mesh \mathcal{M}_m no further FE evaluation is required since $\epsilon_{NM} \approx \widehat{\epsilon}$. Note that this approach to the calibration of the reduced model is parameterless, since the 10% of error comes from the enforcement of a lesser order of magnitude.

5.2 Link of the uncertainty and discretisation error

With the PCE approximation under control, a decision mechanism is required to ascertain whether any of the remaining errors must be further reduced. Due to the generalist aim of our approach, the non-dimensional parameter ε_σ must be defined. This parameter represents the acceptable accuracy in the discretisation error for the QoI and its quotient by the standard deviation relates it with its forwarded uncertainty. When comparing the actual distribution of this error with its acceptable limit ($\widehat{\varepsilon}_\sigma$ in equation 29 compared with ε_σ) at the m -th mesh refinement step, the possible choices for the mechanism are (i) further refinement of the mesh is needed, (ii) the desired accuracy has been achieved, or (iii) more sample evaluations are required to reduce the uncertainty.

Neither $\overline{\mathcal{E}}[\widehat{Q}]$ and $\overline{\mathcal{E}}[Q^h]$ nor any percentile of \widehat{Q} and Q^h are deterministic (these measures were selected in section 4.1 to describe the coarse and fine stochastic fields). In fact, MC sampling approximation turns them into dependent random variables. Let the integer b be an index denoting a pair of outcomes $\overline{\mathcal{E}}[\widehat{Q}]_b$ and $\overline{\mathcal{E}}[Q^h]_b$. Then, the dependent samples producing these outcomes are the sets $\widehat{\mathcal{Q}}_b = \{\widehat{Q}_1, \dots, \widehat{Q}_{ns}\}$ and $\mathcal{Q}_b^h = \{Q_1^h, \dots, Q_{ns}^h\}$, where ns is the number of intermediate outcomes \widehat{Q}_s and Q_s^h corresponding to the same primary samples μ_s . Despite any set indexed by b derives from a specific collection of different aleatory primary samples, the number ns remains constant for all of them.

Prior to describing the refinement indicator (sections 5.2.3 and 5.2.4), section 5.2.1 will introduce the bootstrapping technique to approximate the n_b samples, and section 5.2.2 will be devoted to showing how each of them affects the PDF of the quantities of interest. This will highlight the need of the aforementioned indicator.

5.2.1 Bootstrapping

The uncertainty in the measures $\overline{\mathcal{E}}[\widehat{Q}]$ and $\overline{\mathcal{E}}[Q^h]$ (and percentiles $\overline{\mathcal{C}}_i[\widehat{Q}]$ and $\overline{\mathcal{C}}_i[Q^h]$) is assessed by bootstrapping technique [62, 63]. The technique ensures that the dependent variable variance (obtained through original different computed sets of intermediate outcomes) can be equivalently reproduced through alternative aleatory sets (assembled re-using the already computed intermediate outcomes of the initial set). Diversity on the alternative sets is achieved allowing repetition, decreasing the number of samples in the set or computing some extra intermediate outcomes.

As illustrative example, let the goal be to assess the variance of a dependent response variable $Q := \mathcal{E}[Q^h]$, and the sets of intermediate outcomes Q_s^h used to compute an outcome Q_b prescribed to have 5 components. Then, $Q_b = \overline{\mathcal{E}}[\mathcal{Q}_b] = \overline{\mathcal{E}}[\{Q_s^h\}_{s=1+5(b-1)}^{s=5+5(b-1)}]$ and the first set $\mathcal{Q}_{b=1} = \{Q_s^h\}_{s=1}^{s=5}$. The second set $\mathcal{Q}_{b=2} = \{Q_s^h\}_{s=6}^{s=10}$ can be replaced with an alternative set $\mathcal{Q}_{b^*=2} = \{Q_4^h, Q_1^h, Q_4^h, Q_5^h, Q_1^h\}$ constructed randomly from the first set allowing repetition. Analogously, subsequent sets can be replaced avoiding further model evaluations $Q_{s>5}^h$. This has no impact on the estimation of the variance of Q .

In this work, the Confidence Level (CL) on measures $\overline{\mathcal{E}}[\widehat{Q}]$ and $\overline{\mathcal{E}}[Q^h]$ is determined by means of Confidence Intervals (CI) estimated from the bootstrapped distribution. Due to the peaks on the QoI when a primary sample brings the structure close to resonance, our particular approach to obtain CI is non-symmetric and centred around the median of the bootstrapped PDF. Specifically, for a given number of bootstrapped sets n_b the left and right subintervals (CL_{left} and CL_{right} respectively) forming the CI corresponding to a given confidence level of $CL\%$ reads

$$CI_{left}^{\overline{\mathcal{E}}[Q^h]} := \left[\overline{\mathcal{C}}_{(50-CL/2)}(\overline{\mathcal{E}}[\{\mathcal{Q}_{b^*}^h\}_{b^*=1}^{b^*=n_b}]), \text{median}(\overline{\mathcal{E}}[\{\mathcal{Q}_{b^*}^h\}_{b^*=1}^{b^*=n_b}]) \right], \quad (28a)$$

$$CI_{right}^{\overline{\mathcal{E}}[Q^h]} := \left[\text{median}(\overline{\mathcal{E}}[\{\mathcal{Q}_{b^*}^h\}_{b^*=1}^{b^*=n_b}]), \overline{\mathcal{C}}_{(50+CL/2)}(\overline{\mathcal{E}}[\{\mathcal{Q}_{b^*}^h\}_{b^*=1}^{b^*=n_b}]) \right], \quad (28b)$$

where $\overline{\mathcal{C}}_{(i)}(\cdot)$ denotes the i -th discrete percentile and $[\cdot, \cdot]$ a closed interval.

Even though the CI distance $CI^{\overline{\mathcal{E}}[Q^h]} = CI_{left}^{\overline{\mathcal{E}}[Q^h]} \cup CI_{right}^{\overline{\mathcal{E}}[Q^h]}$ is computed “non-symmetrically centered” around the median, in the figures it will be plotted around the QoI (which is the expectation).

5.2.2 How finite element refinement and addition of samples affect the distribution

Plot contents. The plots in this subsection graphically show the PDF of \widehat{Q}_{PC} and Q_{PC}^h . They also show that they differ due to the difference between the spaces $\widehat{\mathcal{U}}$ and \mathcal{U}^h . Standard Kernel Density Estimation (KDE) was used for estimating these PDFs. The PDFs are included for illustration purposes only since they do not play a role in the algorithm. Within these plots, the graphical representation of the discretisation error $\widehat{\epsilon}$ is the distance $\overline{E}[\widehat{Q}_{PC}] - \overline{E}[Q_{PC}^h]$ (as defined in equation 23). Regarding the graphical representation of the MC sampling error $\bar{\epsilon}$, it is included through the confidence intervals (CI) of these expectations [57] estimated using bootstrapping (see section 5.2.1).

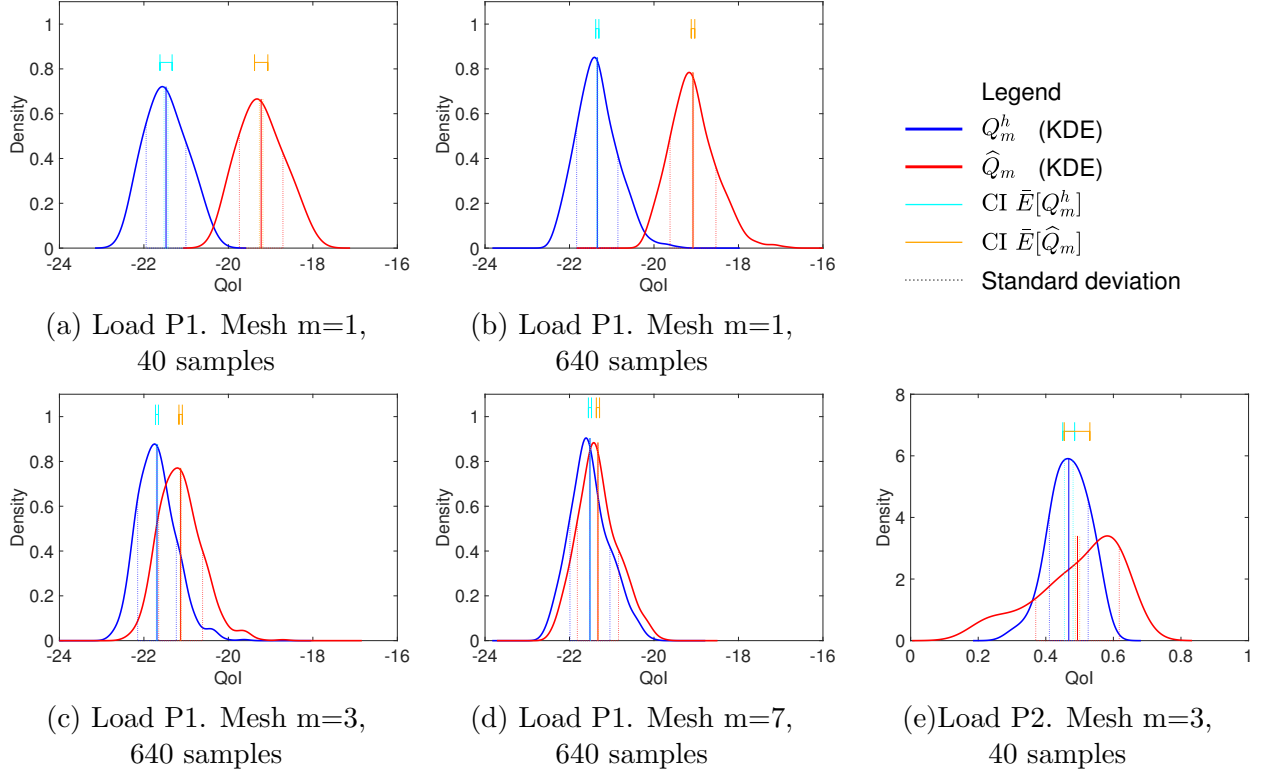


Figure 2: KDE approximation of Q_m^h and \widehat{Q}_m (equation 9) and evolution depending on the number of samples and stages of local mesh refinement. Confidence intervals CI for its expectation computed through bootstrapping

Effects of reducing MC error. Figures 2.a,b show that for a given mesh \mathcal{M}_1 , CI intervals become thinner as we increase the number of samples. This is due to the improved characterisation of the PDF coming from the increase of samples. In contrast, the distance between the estimated expectations is constant, since the discretisation error $\widehat{\epsilon}$ is only improved by refining the mesh. By looking at figures 2.a,b it is immediately noticed that FE refinement is needed for mesh \mathcal{M}_1 , since the discretisation error is much larger than the CI representing the MC error.

Effects of reducing discretisation error. Figures 2.b,c,d show the opposite case. The size of the CI remains of the same order of magnitude if the same number of samples is used in different meshes. On the other hand, the distance between both PDFs and hence their expectation become closer with each mesh refinement.

Need of an specific indicator of refinement. The plots 2.a-d were produced for the loading case P1 (see figure 1). In loading case P1 the parametric uncertainty has a minor contribution to the QoI. It is clear in all the plots that the distance $\overline{E}[\widehat{Q}_{PC}] - \overline{E}[Q_{PC}^h]$ exceeds the CI measuring MC error, even considering the best case within the two sets of CI.

On the other hand, figure 2.e, produced for the loading case P2, shows a case where the confidence intervals overlap. In that case the plot does not provide enough information to establish whether or not the FE error dominates with the required certainty. Either of the errors could predominate considering all possibilities of $\overline{\mathcal{E}}[\widehat{Q}_{PC}]$ and $\overline{\mathcal{E}}[Q_{PC}^h]$ within their CI.

5.2.3 Mechanism to ascertain whether any of the errors must be further reduced

Once established the interaction between the errors and the reduction of uncertainty, a mechanism to unequivocally provide the algorithm with the optimal direction must be formulated. Since the FE discretisation error extended to the parameter space has been defined as the difference $\widehat{\epsilon} = \overline{\mathcal{E}}[\widehat{Q}_{PC}] - \overline{\mathcal{E}}[Q_{PC}^h]$, the logical step is to look at the distribution of the difference rather than looking at both distributions separately. This will avoid overlapping of confidence intervals in figure 2.e.

A stopping criterion as problem independent as possible to accept or reject this error is also required as well as a limit determining the confidence levels for acceptance or rejection.

Regarding the stopping criterion, the common strategy of non-stochastic problems is to define a maximum relative error ε_{FE} for the relative discretisation error $\widehat{\epsilon}_j$ reading $|\overline{\mathcal{E}}[\widehat{Q}_{PC}] - \overline{\mathcal{E}}[Q_{PC}^h]|/|\overline{\mathcal{E}}[Q_{PC}^h]|$. This may suffice in some engineering problems, for instance if a structure is allowed to enter sporadically in the plasticity regime, but not if the interest is in knowing if a crack has formed in a concrete structure. Even in cases where the maximum relative error suffices, it requires a profound understanding of the problem to centre the expectation on a meaningful stochastic measure of the QoI since the statistical variation from it is not taken into account.

We propose a stopping criterion where the discretisation error is normalised by means of the standard deviation $std(\cdot)$. This approach focuses in approximating the area below the PDF rather than the error in the expectation. In this case the user defined limit ε_σ is compared to the relative deviation index reading

$$\widehat{\epsilon}_\sigma := \frac{|\overline{\mathcal{E}}[\widehat{Q}_{PC}] - \overline{\mathcal{E}}[Q_{PC}^h]|}{std(Q_{PC}^h)}, \quad (29)$$

where $std(Q_{PC}^h)$ must be evaluated from the set of outcomes $\{Q_{PC,1}^h, \dots, Q_{PC,n_s}^h\}$. This error can be read as how good is the discretisation error in a QoI with respect its variation, so it is completely problem independent. However, a discrete estimation of the standard deviation is much more sensitive to the lack of samples than a discrete approximation of the expectation. Consequently unless a surrogate model with negligible cost is used, the criterion based on $\widehat{\epsilon}_\sigma$ highly increases the computational cost with respect to the one based on $\widehat{\epsilon}_j$.

Regarding the confidence level (CL), the certainty in the achievement of the desired accuracy will be assessed by percentiles C_{CL}^σ and C_{100-CL}^σ which are defined as percentiles of the bootstrapped distribution of the relative deviation index $\widehat{\epsilon}_\sigma$.

For instance figure 3 contains a case where the confidence level CL^σ was set to 95%, and the desired accuracy to $\varepsilon_\sigma = 0.5$ (which means that the error in the QoI is half the standard deviation, *i.e.* $\widehat{\epsilon}_\sigma < \varepsilon_\sigma = 0.50$ with $CL^\sigma = 95\%$).

In figure 3.a the desired accuracy for the fifth refined mesh lays between the percentiles, implying that it can not be predicted if the outcome for any new set of the same number of sampling points n_s will exceed or fall behind the desired accuracy. In other words, the dominating error is due to lack of sampling and therefore uncertainty must be reduced by increasing the discrete sample population.

Conversely, increasing the number of samples leads to figure 3.b, where the desired accuracy lays on the left side of the percentile $C_{(100-CL)^\sigma}$. Therefore, for the fifth mesh, the likelihood of the error exceeding the desired accuracy ($\widehat{\epsilon}_\sigma > \varepsilon_\sigma = 0.50$) is larger than 95%, when considering at least n_s samples. Then, it can be deduced that discretisation error is predominant and the mesh must be further refined. The reduction of the discretisation error shifts $\widehat{\epsilon}_\sigma$ to the left, so at the end, for a discretised enough mesh, C_{CL}^σ will fall behind $\varepsilon_\sigma = 0.50$ providing certainty that the error in the QoI is smaller than the self imposed limit with a probability of 0.95.

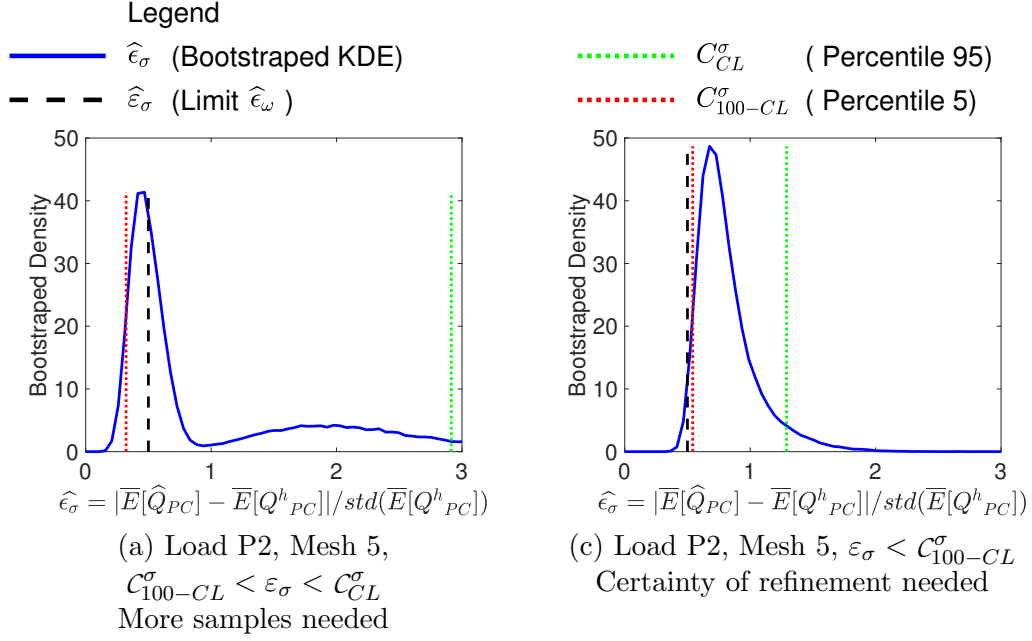


Figure 3: KDE approximation of $\hat{\epsilon}_\sigma$

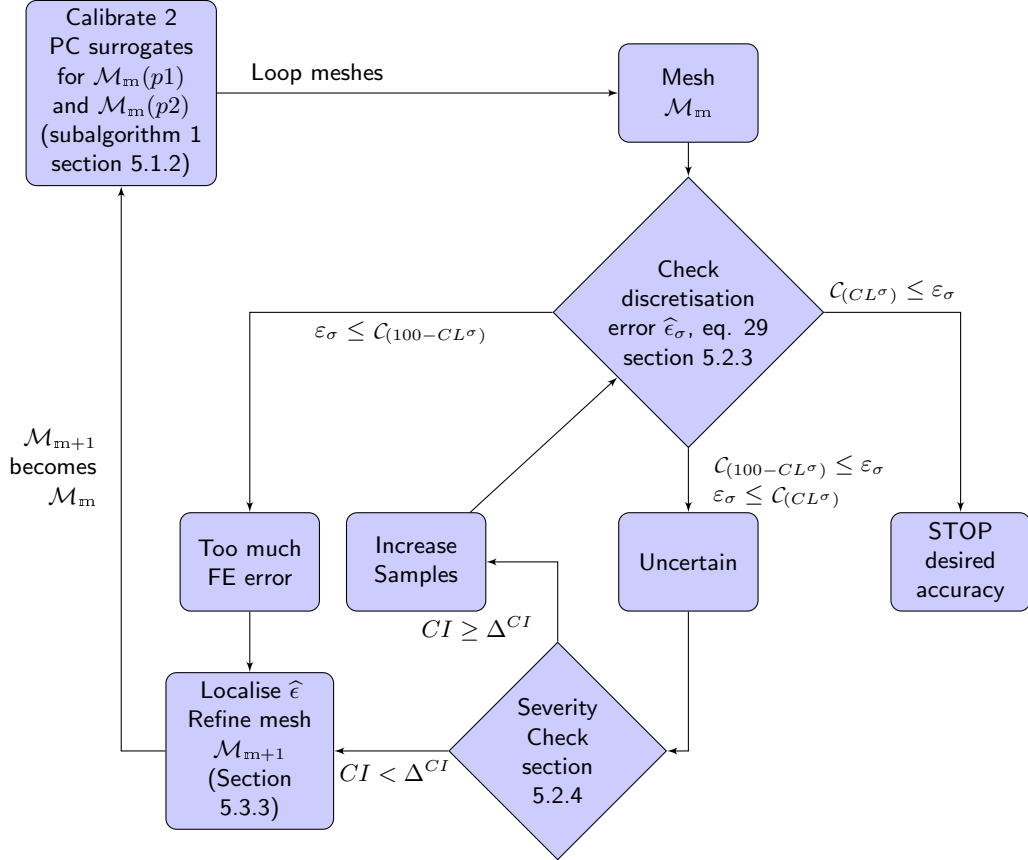


Figure 4: Algorithm map for the criterion based on the discretisation error normalised by the standard deviation

5.2.4 Algorithm map and severity of the certainty assessment

As presented in previous sections, the algorithm might require an unduly large number of evaluations if the relative deviation index equals $\hat{\epsilon}_\sigma$ almost exactly at any point in the refinement process. Only in that case and depending on the surrogate model, the computational cost to reduce the uncertainty enough to facilitate a decision can overcome the cost of arriving at the same conclusion with a refined

mesh. In order to avoid this artificial numerical stagnation, a parameter Δ^{CI} is introduced as a measure of the severity imposed to the stochastic sub-loop.

If the algorithm decides that more samples are needed, before doing so, the parameter controls that the CI is not too small. The distance CI is computed by means of equations 28 and the larger one produced from the coarse and rich spaces is taken into consideration. Then, if $CI < \Delta^{CI}$ it is considered that too much effort has been devoted to sampling and a refinement of the mesh is induced. The belief for this decision is that even if the current discretisation may eventually provide certainty of having reached the final goal, the next discretisation should provide the same certainty with a smaller number of samples. Obviously, because of the computational cost of building the surrogate and evaluating it, to achieve an improvement in computational cost terms, Δ^{CI} should be very strict if the surrogate models are very cheap to evaluate and moderately loose if MC on the original numerical model is used with no surrogate. The final algorithm map including this severity check in the decision of the dominating error is shown in Figure 4.

5.3 Goal-oriented local adaptivity

Once “when to refine” is known, the question of “where to” remains. The QoI is a global quantity so it does not help in deciding where to refine. Consequently, a localised quantity derived from the QoI must be obtained, which is not a trivial task.

Prior to proceeding to define the indicators of refinement, notation for the FEM splitting of any discrete field using the shape functions is due. Let us denote ψ^h and $\hat{\psi}$ as the sets of shape functions associated with spaces \mathcal{V}^h and $\hat{\mathcal{V}}$ respectively. Then, any field $\bullet^h \in \mathcal{V}^h$ can be described as the product between the vector of weights hereafter denoted as $[\bullet^h]$ and the corresponding shape functions ψ^h . Equivalently a field in the fine space $\hat{\bullet} = [\hat{\bullet}] \hat{\psi}$.

5.3.1 Indicators based on the magnitude of the error

A naive approach to defining an indicator of refinement would be to directly use the restriction of the discrete version of equation 17 to the subdomain Ω_k as indicator of refinement for the element e^k . We will use the nomenclature ‘direct’ to refer to this indicator, as well as the symbol $\hat{\eta}_k^D$. Using the rich and coarse spaces $\hat{\mathcal{V}}$ and \mathcal{V}^h it reads

$$\hat{\eta}_k^D := \mathcal{R}_{\Omega_k}^\omega(\hat{z}) = a_{\Omega_k}^\omega(\hat{e}, \hat{z}). \quad (30)$$

Due to Galerkin orthogonality, the residual of any field $\zeta^h \in \mathcal{V}^h$ is zero (*i.e.* $\mathcal{R}^\omega(\zeta^h) = 0$). So it is possible to modify equation 30 to compute the orthogonal part with respect to the coarse space \mathcal{V}^h . Despite the localised contribution to the QoI $\hat{\eta}_k^\perp$ will change, the global QoI will remain unaffected.

$$\hat{\eta}_k^\perp := \mathcal{R}_{\Omega_k}^\omega(\hat{z} - z^h) = a_{\Omega_k}^\omega(\hat{e}, \hat{z} - z^h). \quad (31)$$

An indicator based on localisation of the mass norm was defined, with the only purpose of showing that all the localised indices point to where the error is larger and that this is not useful to drive the refinement strategy. The indicator based on the mass matrix reads

$$\hat{\eta}_k^{MN} := \rho \cdot \omega^2 \int_{\Omega_k} \left([\hat{e}]^T \hat{\psi} \cdot \hat{\psi} [\hat{e}] \right) d\Omega, \quad (32)$$

where the error field \hat{e} in the fine space $\hat{\mathcal{V}}$ has been decomposed using the corresponding shape functions $\hat{\psi}$.

It is clear that for the posed problem, the indicator $\hat{\eta}_k^{MN}$ will always point to the top part of the structure, since it is where the displacement and the error are larger (see horizontal deformation in figure 5). The indicators based on the QoI introduce the sensitivity field z which modifies this focus (lighter areas in figure 5.a have more influence), but they are still based on the magnitude of the error. Section 5.3.4 will show that this leads to very poor refinement strategies.

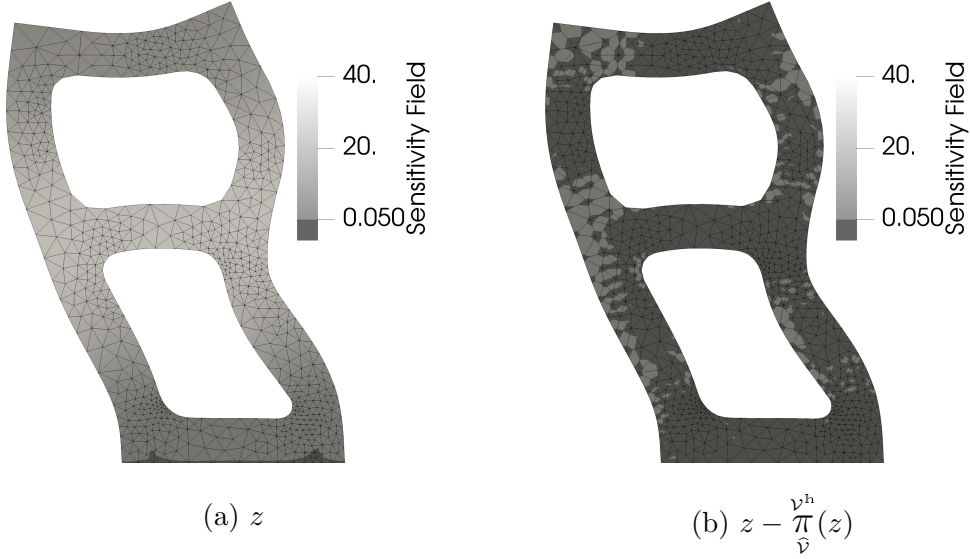


Figure 5: Sensitivity fields for the QoI, load P1, ω between 1st and 2nd natural frequency

5.3.2 Indicators based on the variation of the error

Refinement indicators based on the energy norm usually lead to excellent convergence. Due to the definition of the energy norm, those indicators take into account the gradient. The mentioned indicator reads

$$\widehat{\eta}_k^{EN} := a_{\Omega_k}^\omega(\widehat{e}, \widehat{e}). \quad (33)$$

Including the gradient in the indicator means that it points to where the error changes the most, so where there is more probability of improvement.

The goal is then to define an indicator of refinement $\widehat{\eta}_k^\partial$ based on the QoI that points to the elements where the error varies the most, and not where it is larger as was the case of $\widehat{\eta}_k^{MN}$.

Oden [46] proposes an indicator equivalent to $\widehat{\eta}_k^\partial = \widehat{\eta}_k^{EN} \cdot \widehat{\eta}_k^D$, where one term of the product accounts for influence field and the other for the energy of the system. Another technique is to define a QoI which involves a gradient, e.g. an indicator based on the stress [40]. Later works, as the one by Rognes [64], base the indicator on the equilibrated residual, integration by parts and redistribution of the normal derivative which accounts for the contribution of the rest of the domain in the element e^k .

The present work relies on Galerkin orthogonality and the use of p-refinement to achieve the same goal in a much simpler discrete way. The idea is to subtract all the coarse FE component of the error interpolated to the rich space from the influence field. As already mentioned, subtracting any coarse field from equations 17 has no influence on the global QoI but affects the local contributions.

In order to describe the projection field $v^{h*} \in \mathcal{V}^h \subset \widehat{\mathcal{V}}$ of a field $\widehat{v} \in \widehat{\mathcal{V}}$, let us denote i_{DOF} as the i^{th} degree of freedom of any coarse field and n_{DOF} as the total number of degrees of freedom determined by the FE coarse mesh. Effectively, this index points to a component of the vector of weights $[v^{h*}]$, and to position $\mathbf{x}_{i_{\text{DOF}}}$ in the material space (\mathbb{R}^d) which is independent of the functional space (\mathcal{V}^h or $\widehat{\mathcal{V}}$). Then,

$$v^{h*} := \frac{\nu^h}{\hat{\nu}}(\widehat{v}) \quad (34)$$

where the projector operator $\frac{\nu^h}{\hat{\nu}}(\cdot)$ is such that

$$\frac{\nu^h}{\hat{\nu}}(\widehat{v}) : [v^{h*}]_{i_{\text{DOF}}} = \widehat{v}(\mathbf{x}_{i_{\text{DOF}}}) \quad \forall i_{\text{DOF}} \in \{1, \dots, n_{\text{DOF}}\} \quad (35)$$

Therefore, the proposed indicator based both on the variation of the error and the influence field reads

$$\widehat{\eta}_k^\partial := \mathcal{R}_{\Omega_k}^\omega(\widehat{z} - \frac{\nu^h}{\widehat{\nu}}\pi(\widehat{z})) = a_{\Omega_k}^\omega(\widehat{e}, \widehat{z} - \frac{\nu^h}{\widehat{\nu}}\pi(\widehat{z})). \quad (36)$$

Figure 5.b clearly shows that by removing completely any contribution belonging to \mathcal{V}^h , the only local contributions to the global QoI are those where the p2 shape functions capture better the error than the p1 shape functions. Indeed, these contributions are larger where the error varies the most, which was the goal in the first place.

5.3.3 Local mesh refinement strategy adopted

All indicators defined on sections 5.3.1 and 5.3.2 try to estimate which elements contribute the most to the error, not the error per se. In all cases, the local refinement strategy consists of sorting elements from largest to smallest and marking elements for refinements until a 10% of the sum of indicators.

Technically, for the indicator $\widehat{\eta}_k^\partial$, the set of sorted elements forming mesh \mathcal{M}_m reads $\mathcal{E}_s = \{\mathbb{e}_{ks}\}_{ks=1}^{ks=n_e}$ such that

$$ks_j < ks_k \Leftrightarrow \widehat{\eta}_{ks_j}^\partial \geq \widehat{\eta}_{ks_k}^\partial \quad \forall j, k \quad (37)$$

Then, the set of elements marked for refinement $\mathcal{E}_R \subset \mathcal{E}_s = \{\mathbb{e}_{ks}\}_{ks=1}^{ks=n_e}$ is defined satisfying

$$\begin{aligned} \sum_{\substack{ks=1 \\ ks=n_{e_R}}}^{ks=n_{e_R}-1} \widehat{\eta}_{ks}^\partial &< 0.1 \cdot \sum_{\substack{ks=1 \\ ks=n_e}}^{ks=n_e} \widehat{\eta}_{ks}^\partial, \\ \sum_{ks=1} \widehat{\eta}_{ks}^\partial &\geq 0.1 \cdot \sum_{ks=1} \widehat{\eta}_{ks}^\partial \end{aligned} \quad (38)$$

Since information has not to be transferred from one mesh to another as in the case of time dependent problems, a non-conforming re-meshing refinement strategy was preferred. In particular the software Gmsh [65] and its option threshold field was used to that purpose. The benefits with respect to the more extended approach of subdividing only the marked elements with and without extra edges are lack of skewed elements and lack of hanging nodes respectively. The only drawback is a slight increase in the number of degrees of freedom with respect to subdividing an element. See figure 6 for visual support on the three types of local refinement cited.

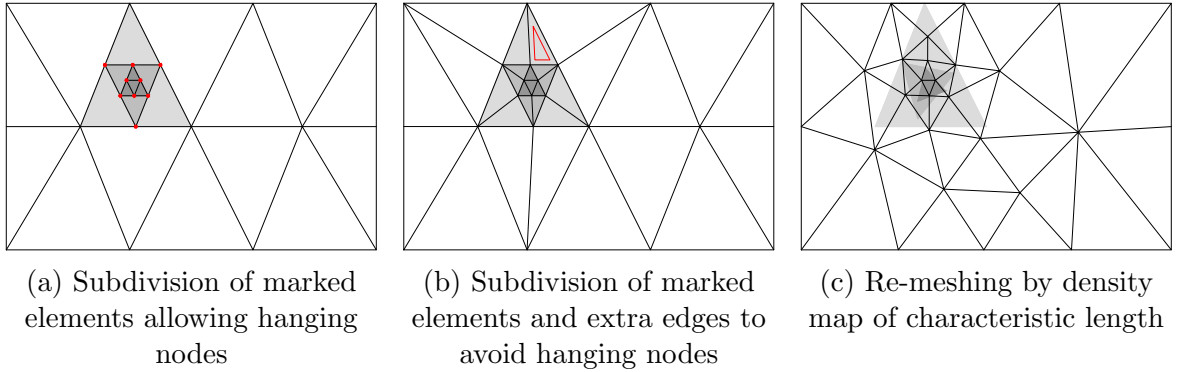


Figure 6: Resulting meshes depending on the refinement strategy after 4 levels of adaptive local refinements

5.3.4 Effectivity of the different indicators of refinement

When the described indicators are applied to the stochastic problem posed, Figure 8 shows that the ones based on the magnitude of the error have poor performance. Indicators $\widehat{\eta}_k^D$ and $\widehat{\eta}_k^\perp$ improve from $\widehat{\eta}_k^{MN}$ because the influence field weights the new area of interest farther from the top, where the magnitude of the error is larger.

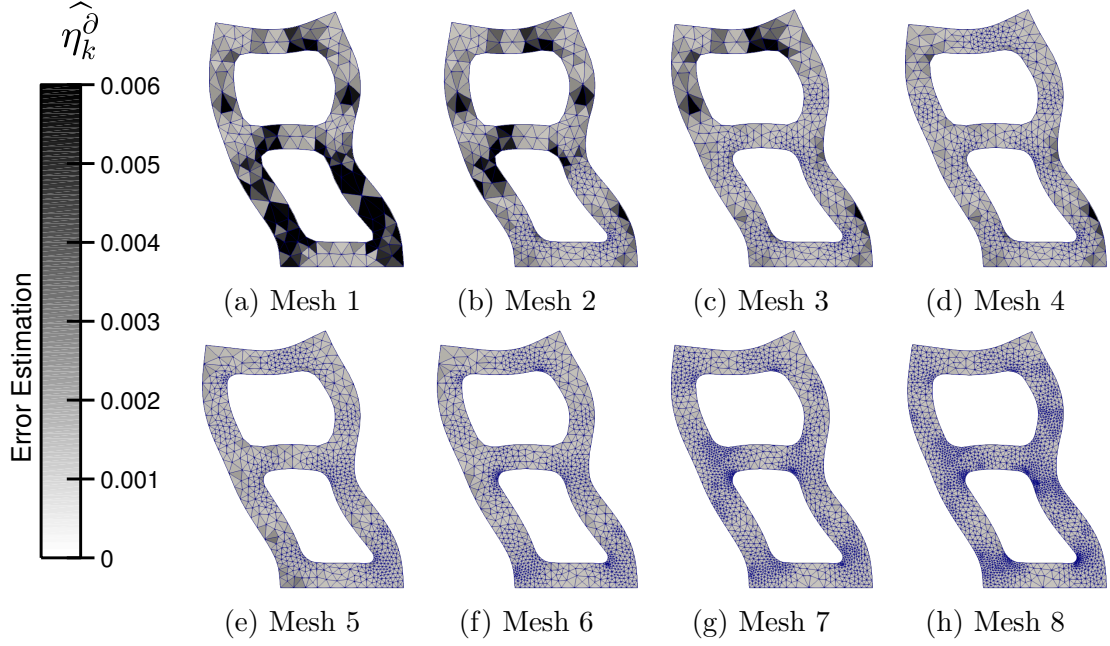


Figure 7: Evolution of the mesh refinement for load case P1, based on criterion 38

On the contrary, indicators based on the variation of the error $\widehat{\eta}_k^{EN}$ and $\widehat{\eta}_k^\partial$ converge faster than uniform refinement. Obviously, convergence for the global energy norm using $\widehat{\eta}_k^\partial$ is worse than just using local energy norm ($\widehat{\eta}_k^{EN}$) as indicator of refinement, although they are close. Nevertheless, $\widehat{\eta}_k^\partial$ is a specialised indicator that leads to better results than $\widehat{\eta}_k^{EN}$ for the QoI, because it still has the influence field, even if it is equal to zero in the nodes belonging to the coarse space.

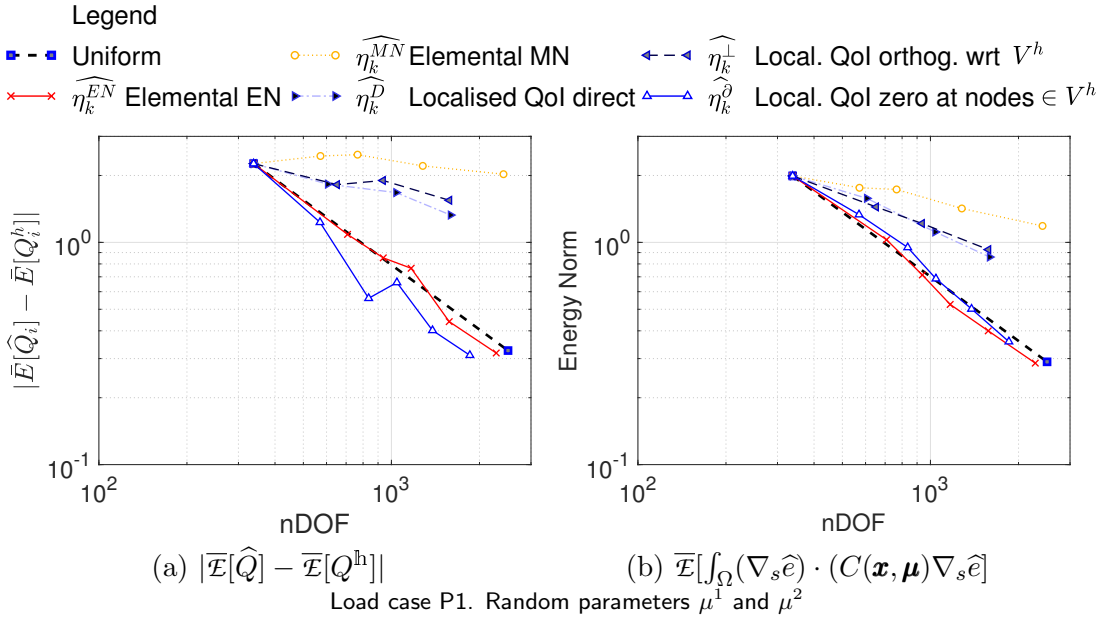


Figure 8: Convergence depending on the refinement criteria

5.3.5 Concentration of refinements check

The benefits of localisation of refinement is usually presented with diffusion or flow over a notch problems which leads to high concentration of the mesh refinement around the notch or the source.

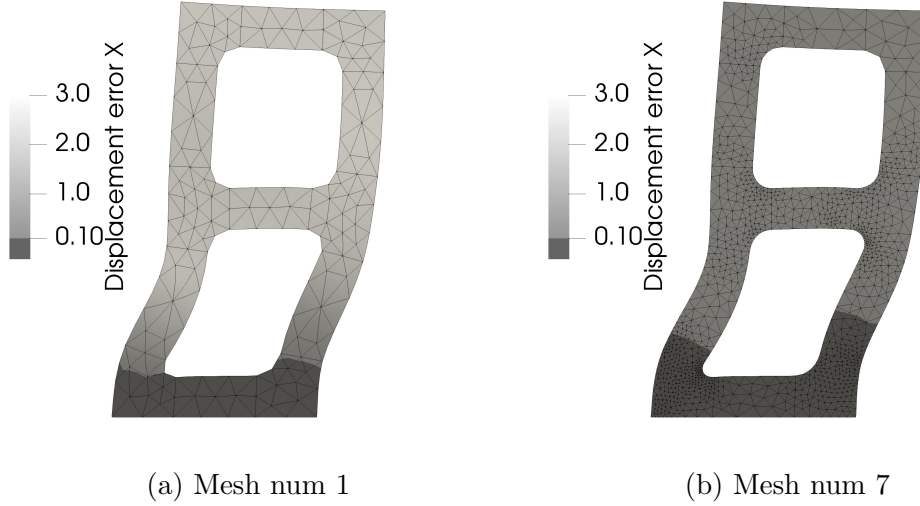


Figure 9: Concentration of refinements in the lower part for the case load P3 and $\omega = 0$
Error in X displacement is plotted at each nodes from $\hat{e}_m = \hat{u}_m - e_m^h$ ($m = \text{meshes 1 and 7}$)

On the other hand, the goodness of concentration of local refinements is not as acute for structural vibration problems, since displacements and hence errors due to harmonic loads tend to propagate. In addition, the placement of these refinements is not always intuitive to check. Nevertheless, the ability to capture these local phenomena is needed to validate a refining indicator. As a consequence, the case of load P3 and $\omega = 0$ was introduced as a test for the refinement indicator.

In this test the natural frequencies are almost not excited. Then, if both the load P3 and the domain Ω_{Q3} are defined in the lower part of the structure, there should be concentration of refinement on this lower part. Results in Figure 9 shows an acute concentration of refinement at stage 7. Therefore, considering the good convergence and the ability to concentrate refinements we can conclude that, from the presented indicators, $\widehat{\eta}_k^\partial$ is the most suitable to lead the goal-oriented refinement process.

6 Numerical results

Based on the problem defined in section 3, the present section includes the numerical results for three different loading cases. The geometry and parameters for the structure are listed next. $L=1$, $R=0.1$, $T=0.2$, $P1=P2=P3=1/\text{length unit}$, $\boldsymbol{\mu} = \{\mu^1, \mu^2\}$ following the normal uncorrelated distribution $\mathcal{N}([0.5 ; 0.7], [0.3^2, 0 ; 0, 0.3^2])$, $\rho = 1$ and $\omega = 0.3$ (between the first and the second natural frequency).

The results are structured in 3 subsections devoted to check the 3 different sources of error described in section 4.3.

6.1 Results for the surrogate model

The first loading case P1 consists of a horizontal load that excites first and second natural frequencies in a direct manner. Furthermore, the QoI (defined as average of the horizontal displacement in one tip corner) is also very influenced by a direct horizontal load. Even though both parameters have also impact on the QoI, this impact is in general minor compared to the load contribution.

Figure 10a,b shows that the error in the QoI is reduced globally in all the parameter domain where samples are approximated. We see that for load P1, order 3 Hermite polynomials are accurate enough to keep polynomial chaos error below the discretisation error even for 9th stage refinement meshes. Recall that subalgorithm 1 is used to fit two different PCE for each mesh (See equations 26 and 27 where the surrogate models are fitted to reproduce the original FEM models for each mesh). The strictly incremental iterative increase in accuracy strategy for the PC surrogate model defined in section 5.1.2 comes from the fact that more accurate meshes produce less discretisation error.

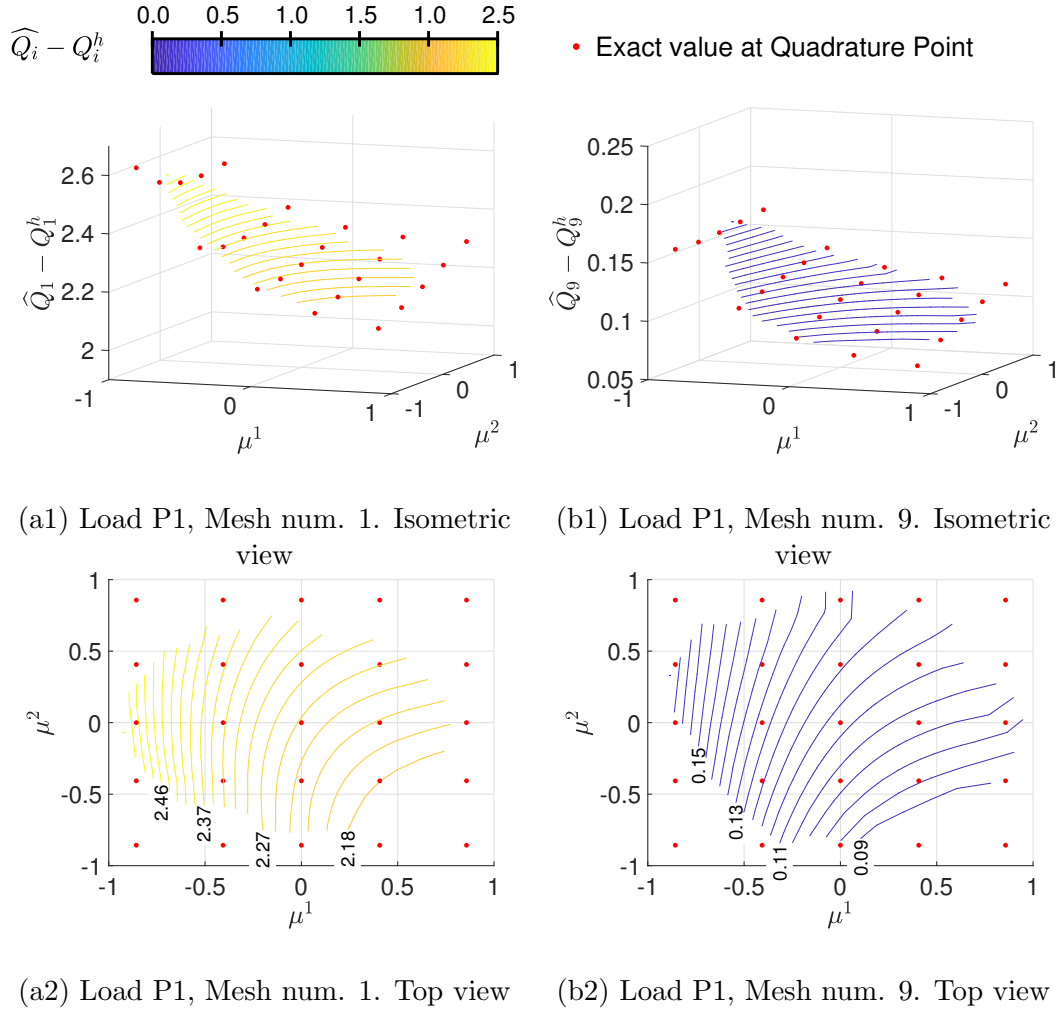


Figure 10: Parameter response surface ‘error in the QoI’

Therefore, errors introduced by a low order PCE may become of the same order than the difference between next iteration of refined meshes, but not the opposite.

The second loading case is a vertical one. In contrast to the previous case, parameter variation is now the only factor that significantly affects the QoI. Consequently, the parameter surface equals zero when the parameters are also zero. Parameter zero means Young’s modulus equals 1 which is the same for the rest of the structure.

Surface plots show similar results except for the fact that an increasing number of polynomials is needed to keep the error below the discretisation error. Figure 11a-d show slices of the parameter surfaces through lines of quadrature points so that direct computations can be included.

It is interesting to notice that as the complexity of the parameter surface increases the quadrature points cover a wider area, even farther than the high probability sampling area that defined the polynomials on the first place. Of course, by increasing infinitely the number of samples, eventually the sampling area will overcome the area covered by the quadrature points regardless of their order.

Although only the central and one of the extreme slices in μ^1 direction have been included in figure 11a-d, it can be seen that the error of the polynomial chaos approximation is larger the farther we are from the mean of the sampling distribution (in our case $\mu^1 = \mu^2 = 0$ corresponding to Young’s moduli =1). While the values close to this mean fit almost perfectly, approximations in the extremes do not perform so well. This behaviour was to be expected because even if the fitting process ensures that the error is minimized with an exact integration in the whole infinite parameter domain, the weights considered in the integration quadrature enhance contributions of the maximum probability region.

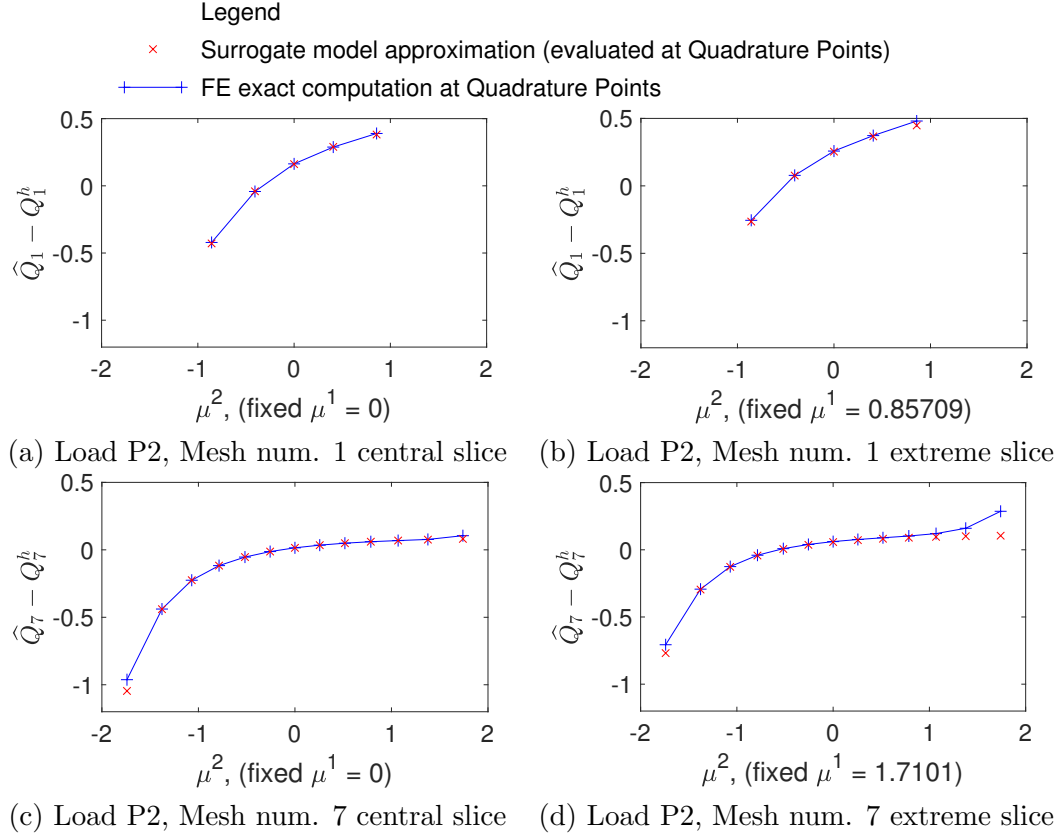


Figure 11: Slices of the parameter response surface ‘error in the QoI’ (equivalent to figure 10 for load P2)

6.2 Discretisation convergence

Regarding the discretisation error, which drives the problem and serves as reference for the rest of errors, the convergence of the QoI is the best way to assess its accuracy. The whole point of adaptive refinement is to obtain a lesser error than uniform refinement for the same number of degrees of freedom so that computational time is saved.

The error at each step in figures 12.a-d is estimated as the difference between the expectation of the QoI using linear and quadratic elements ($\overline{\mathcal{E}}[Q_m^h]$ and $\overline{\mathcal{E}}[\widehat{Q}_m]$) for the given mesh \mathcal{M}_m . In order to rule out the possibility that results are polluted due to mesh dependence of the estimations, the same errors were computed as the difference between the coarse solution $\overline{\mathcal{E}}[Q_m^h]$ at each mesh and a fixed reference solution $\overline{\mathcal{E}}[\widehat{Q}]$, with similar results. The mesh producing the reference solution was obtained by taking the finer uniform mesh and marking for refinement all elements adjacent to the curved boundary.

From the computed cases, Figure 8 already shows that this is the case for load P1 where the uncertainty is small. Even though the case of load P2 produces more uncertainty, Figure 12 shows that the better convergence is consistent for a large number of mesh refinements and all considered loading cases. However, the path to convergence has significant oscillations in the second case. Regarding the order of improvement with respect to the uniform refinement, in both loading cases the gain it is of the same order for the static and the $\omega = 0.3$ frequency cases (between first and second natural frequencies).

Results for the computation of percentiles included in figure 13 show that the algorithm performs similarly independently of the probabilistic measure selected, even if it can not be integrated analytically through the surrogate model. Furthermore, the sets of results for the 95th percentile include weighted XY strains, non restricted to mesh-conforming sub-domains as an alternative QoI.

On the matter of the oscillations, they appear due to two facts. In the first place, in load P2 the only reason for lateral displacement is the parameter variation, which makes different samplings

Legend: -■- Uniform refinement — Adaptive refinement (Indicator $\hat{\eta}_k^{\partial}$)

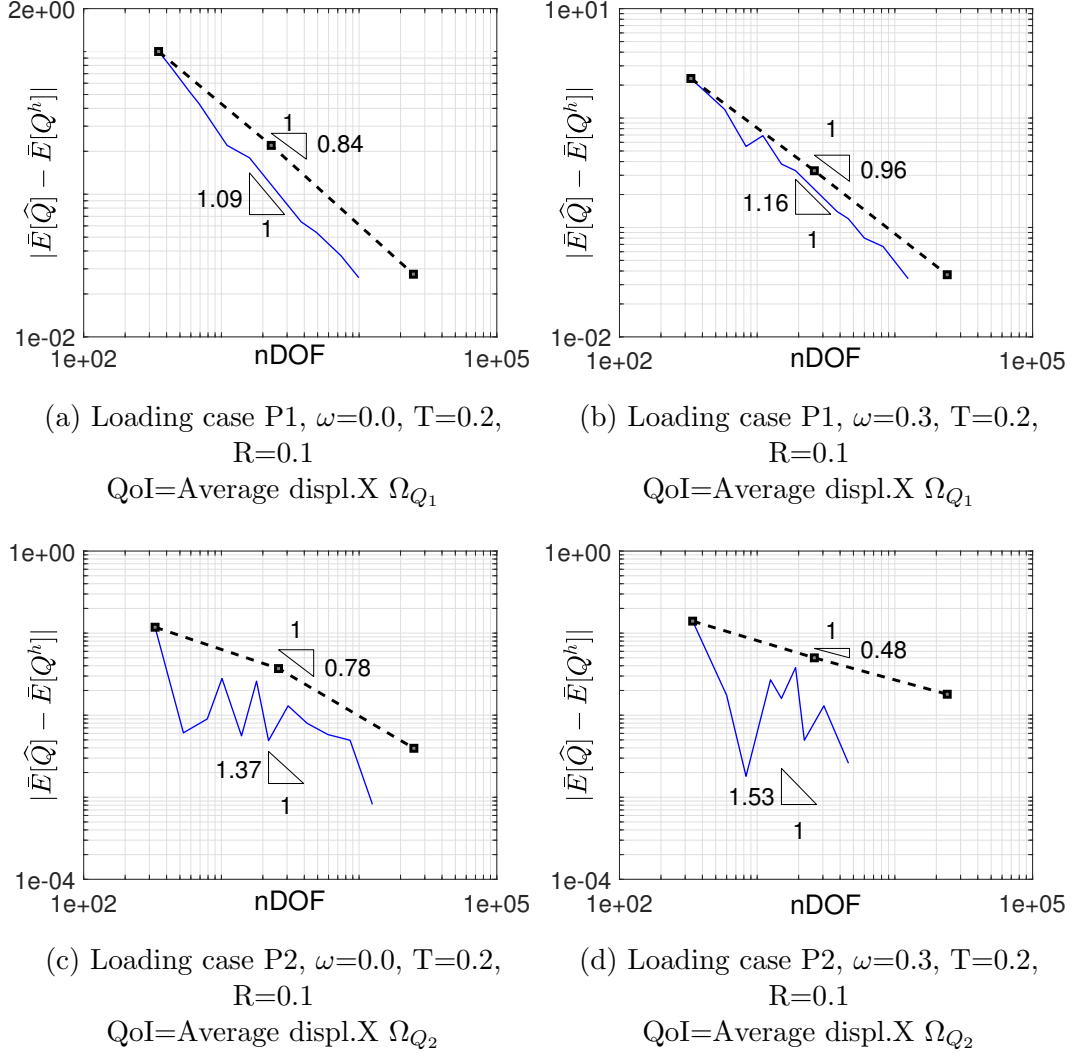


Figure 12: Convergence of $|\bar{E}[\hat{Q}] - \bar{E}[Q^h]|$

Legend: -■- Uniform refinement — Adaptive refinement (Indicator $\hat{\eta}_k^{\partial}$)

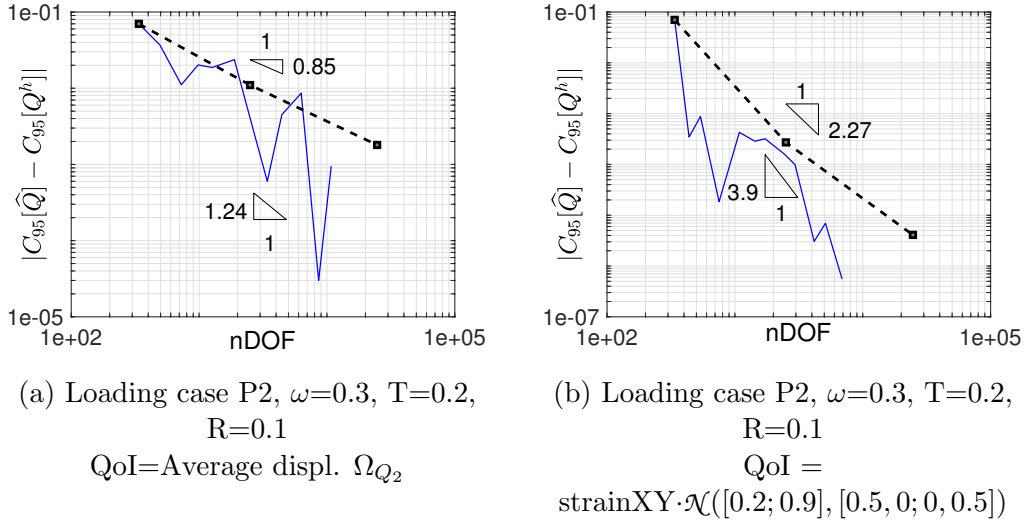


Figure 13: Convergence of $|\bar{C}_{95}[\hat{Q}] - \bar{C}_{95}[Q^h]|$ and alternative quantities of interest

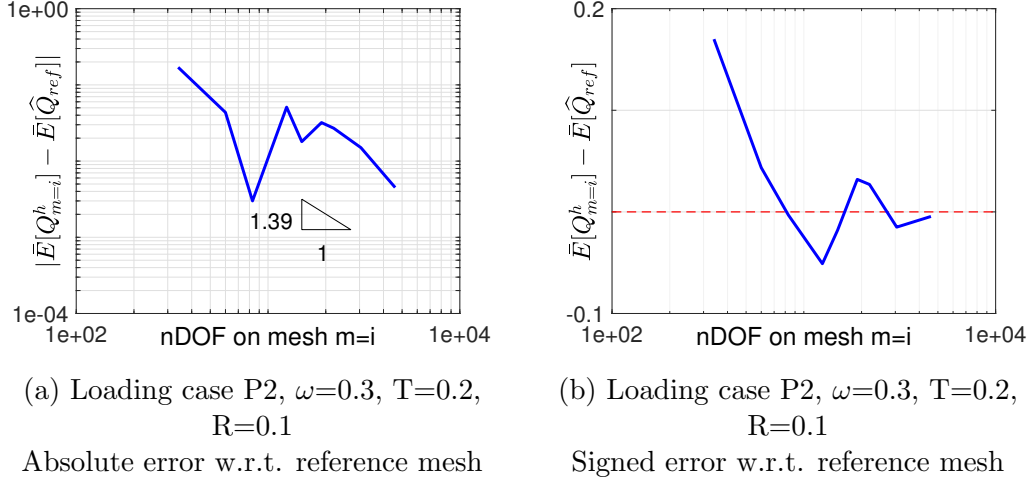


Figure 14: Classic convergence analysis to check the non-computable part of the error $\tilde{\epsilon}$ (see eq.23)

present a much larger discrepancy in the QoI (and hence its error) than load P1 case. Second, a non-uniform mesh has profound impact on the displacement and rotations of the domain introducing an oscillatory component to the general asymptotic evolution of the QoI, and this is inherited by the error measures. Due to geometric constraints, it is not possible to implement a mesh refinement strategy with steps small enough to mitigate this effect. Furthermore, even if it was possible, it will unduly increase the number of meshes to be assessed wasting the increase of computational performance gained with respect to uniform refinement.

Finally, a classic convergence analysis was performed in order to check the assumption made in sub-section 4.3 neglecting the non-computable part of the error. Figure 14 consists of two plots of the evolution of the error between the iterative QoI in the coarse space and a reference solution. On the left we see similar results than the ones obtained in Figure 12.d while in the right, the signed error displays the oscillations mentioned.

6.3 Sampling stop criterion

This section provides evidence that the confidence intervals serve their purpose. In other words the stochastic error due to stop the sampling strategy early is controlled. In order to perform this verification, the problem was computed 34 times allowing randomness in all samplings. The area between percentiles 5 and 95 was used as confidence interval, so an average of 3.4 cases are expected to be outside of the confidence interval at each step of the mesh refinement. Of course, the number of samples is too small in order to have conclusive results or any precision in this average. However, figure 15 shows that even for a small amount of computed cases, the order of magnitude of the confidence intervals is close to 3.4.

Testing all the computed cases, the average for all cases and meshes varies from 1.6 to 4.4. Because of the small number of cases computed, the standard deviation is quite high ranging from 2.5 to 5.4. After checking that the MC expectation of the error in the QoI is controlled through confidence intervals, the final mesh for different sampling strategies was tested. Adapted meshes were included in figure 16 with and without the implementation of confidence intervals and cutting early the sampling process.

It is clear that both sampling strategies lead to almost the same refined mesh. The implementation of confidence intervals is then an excellent tool to save computational time. This is particularly helpful when polynomial chaos is not included in the algorithm, which is a sensible choice if the number of dimensions of the stochastic space is large enough. In this case, the curse of dimensionality makes evaluating the Hermite-Gauss quadrature points really expensive in computational time terms.

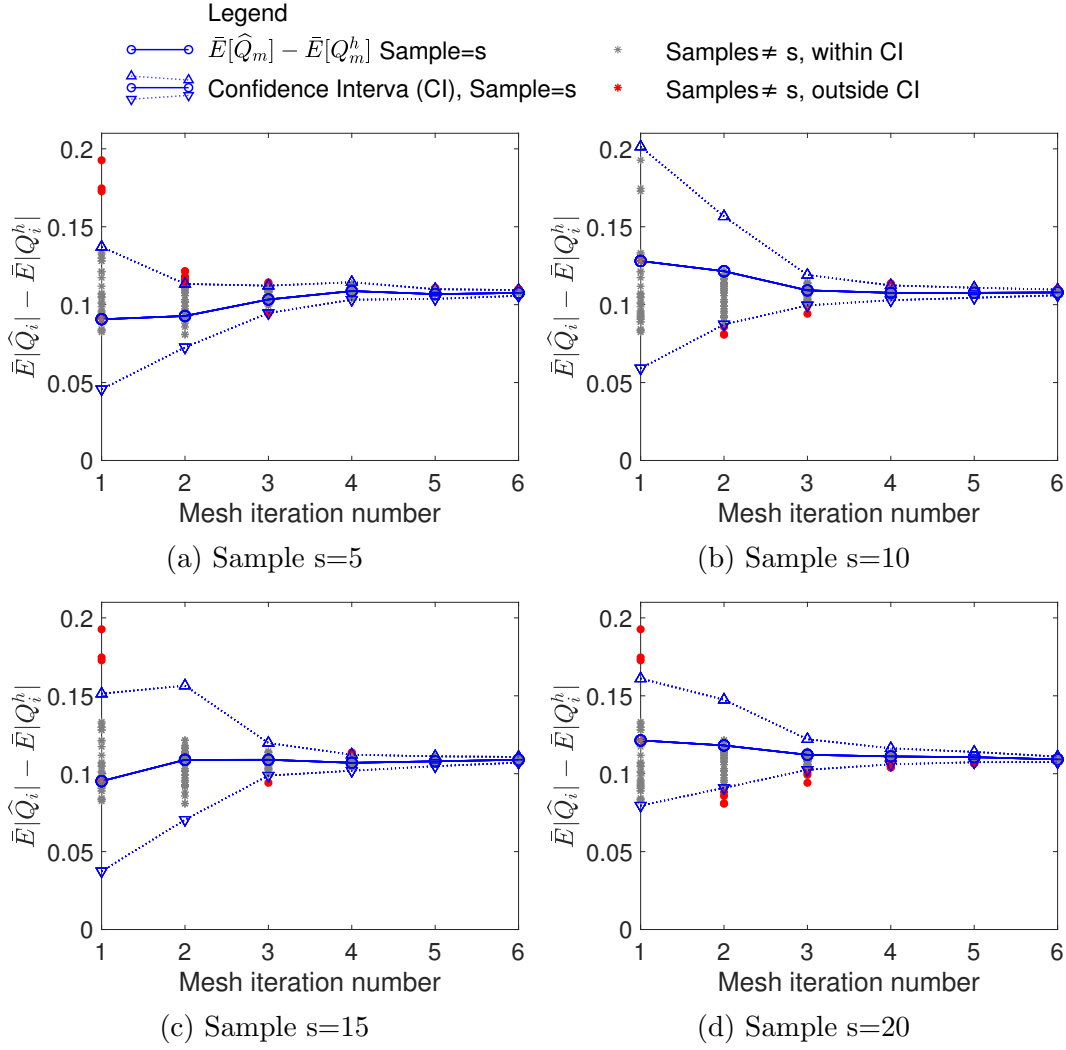
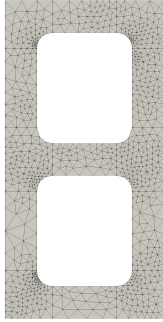
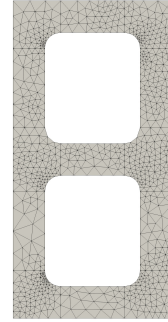


Figure 15: Confidence Interval validation, computed from 4 different samples s



(a) Minimum 160 samples, then check CI



(b) Minimum 40960 samples. No CI implemented

Figure 16: Final mesh for 6 local refinements

Conclusions

Discretisation error and parametric uncertainty can be linked under a single convergence criterion to control the errors in spatial, surrogate and parametric spaces simultaneously. This allows to adaptively refine the spatial discretisation not only to produce an error scaled with the uncertainty, but also to be optimised with respect to any QoI whose probabilistic measures become the unknown random variable dependent of the parameters.

The indicator of refinement needs to be based on where the error varies the most. To that effect,

if p-refinement reference space is used, simply removing all the contribution of the coarse space to the QoI suffices. Furthermore, it leads to an indicator which is similar to the ones based on the energy norm, but that takes the dual weight of the goal-oriented residual into consideration. Any error estimator or indicator can be used as indicator of refinement in place of the approach chosen for this paper where the estimator consists on the difference between the solution using the same mesh with quadratic and linear elements. However, when the QoI does not involve a gradient, the indicator must point to where the error varies the most by any other means.

Results show that the presented algorithm minimises the computational efforts in the spatial discretisation, in the construction of the surrogate and in the MC sampling to characterise the stochastic process. Moreover, an optimal mesh also reduces the computational cost of the model evaluations needed to build the surrogate model or to perform MC sampling if no surrogate model is used.

In this work, the only parametrised quantity is the field of Young moduli. However, all the algorithmic propositions presented in this paper can be applied to parametrised boundary data and mass densities. Excitation frequency ω may also be treated as an adjustable or unknown parameter. Even if the algorithm was tested for a frequency domain elasto-dynamics application, nothing in its formulation limits it to this particular application. The proposed parametric problem is simply a relevant simplified benchmark.

The fundamental contribution of the work consists in a tool that allows to control simultaneously FE discretisation and stochastic errors avoiding undue over-discretisation and therefore minimising the computational cost. The range of applications for this tool includes any method involving sample evaluation of FE models commonly used in structure reliability analysis or crack prediction. Some examples are forward uncertainty propagation, Bayesian inference, sampling methods (importance, adaptive or Latin hypercube sampling) and kriging method.

Acknowledgements

This project has been supported by the Engineering Research Network Wales (Rhwydwaith Ymchwil Peirianeg Cymru) under grant NRN071.

The 1st author also acknowledges Dr. Iulia Mihai and the project "Two-scale numerical simulations for fibre reinforced cementitious composites" funded by EPSRC for their support on the very late stages of the present work.

References

- [1] Berger, M.J., Adaptive Mesh Refinement for hyperbolic differential equations, PhD thesis, Stanford University, 1982.
- [2] Zhu, J.Z. and Zienkiewicz, O.C., Adaptive Techniques in the Finite Element Method., *Commun. Appl. Numer. Methods*, 4(2):197–204, 1988.
- [3] Chen, L. and Rao, S., Fuzzy finite-element approach for the vibration analysis of imprecisely-defined systems, *Finite Elem. Anal. Des.*, 27(1):69–83, sep 1997.
- [4] Babuška, I., Nobile, F., and Tempone, R., Worst case scenario analysis for elliptic problems with uncertainty, *Numer. Math.*, 101(2):185–219, aug 2005.
- [5] Chamoin, L., Díez, P., Maday, Y., Huerta, A., Ladeveze, P., Nadal, E., and Ródenas, J.J., *Verifying Calculations - Forty Years On*, SpringerBriefs in Applied Sciences and Technology, Springer International Publishing, Cham, 1st edition, 2016.
- [6] Ainsworth, M. and Oden, J.T., *A Posteriori Error Estimation in Finite Element Analysis*, John Wiley & Sons, Inc., Hoboken, NJ, USA, 2000.
- [7] Kerfriden, P., Ródenas, J.J., and Bordas, S.P.A., Certification of projection-based reduced order modelling in computational homogenisation by the constitutive relation error, *Int. J. Numer. Methods Eng.*, 97(6):395–422, feb 2014.

- [8] Kahn, H. and Marshall, A.W., Methods of Reducing Sample Size in Monte Carlo Computations, *J. Oper. Res. Soc. Am.*, 1(5):263–278, 1953.
- [9] Bucher, C.G., Adaptive sampling — an iterative fast Monte Carlo procedure, *Struct. Saf.*, 5(2):119–126, jun 1988.
- [10] Babuška, I., Nobile, F., and Tempone, R., A Stochastic Collocation Method for Elliptic Partial Differential Equations with Random Input Data, *SIAM J. Numer. Anal.*, 45(3):1005–1034, jan 2007.
- [11] Bender, C.M. and Orszag, S.A., *Advanced Mathematical Methods for Scientists and Engineers I*, Springer New York, New York, NY, 1999.
- [12] Madsen, H., Krenk, S., and Lind, N., *Methods of Structural Safety*, Dover, Mineola, N.Y., 2006.
- [13] Zhang, J. and Ellingwood, B., Orthogonal series expansions of random fields in reliability analysis, *J. Eng. Mech.*, 120(12):2660–2677, dec 1994.
- [14] Ghanem, R.G. and Spanos, P.D., *Stochastic Finite Elements: A Spectral Approach*, Springer New York, New York, NY, 1 edition, 1991.
- [15] Xiu, D. and Karniadakis, G., The Wiener-Askey polynomial chaos for stochastic differential equations, *SIAM J. Sci. Comput.*, 24(2):619–644, 2002.
- [16] Grigoriu, M., On the spectral representation method in simulation, *Probabilistic Eng. Mech.*, 8(2):75–90, jan 1993.
- [17] Baier, C., D’Argenio, P., and Groesser, M., Partial Order Reduction for Probabilistic Branching Time, *Electron. Notes Theor. Comput. Sci.*, 153(2):97–116, may 2006.
- [18] Kundu, A., Matthies, H., and Friswell, M., Probabilistic optimization of engineering system with prescribed target design in a reduced parameter space, *Comput. Methods Appl. Mech. Eng.*, 337:281–304, aug 2018.
- [19] Mattis, S.A. and Wohlmuth, B., Goal-oriented adaptive surrogate construction for stochastic inversion, *Comput. Methods Appl. Mech. Eng.*, 339:36–60, 2018.
- [20] Oden, J.T., Babuska, I., Nobile, F., Feng, Y., and Tempone, R., Theory and methodology for estimation and control of errors due to modeling , approximation , and uncertainty, *Comput. Methods Appl. Mech. Eng.*, 194:195–204, 2005.
- [21] Chamoin, L., Florentin, E., Pavot, S., and Visseq, V., Robust goal-oriented error estimation based on the constitutive relation error for stochastic problems, *Comput. Struct.*, 106:189–195, 2012.
- [22] Colomés, O., Scovazzi, G., and Guilleminot, J., On the robustness of variational multiscale error estimators for the forward propagation of uncertainty, *Comput. Methods Appl. Mech. Engrg.*, 342:384–413, 2018.
- [23] Almeida, R.C. and Oden, J.T., Solution verification, goal-oriented adaptive methods for stochastic advection- diffusion problems, *Comput. Methods Appl. Mech. Engrg.*, 199:2472–2486, 2010.
- [24] Butler, T., Dawson, C., and Widley, T., A posteriori error analysis of stochastic differential equation using polynomial chaos expansion, *SIAM J. Sci. Comput.*, 33:1267–1291, 2011.
- [25] Liang, B. and Mahadevan, S., Error and uncertainty quantification and sensitivity analysis in mechanics computational models, *Int. J. Uncertain. Quantif.*, 1(2):147–161, 2011.
- [26] Hoang, K., Kerfriden, P., and Bordas, S., A fast, certified and “tuning free” two-field reduced basis method for the metamodelling of affinely-parametrised elasticity problems, *Comput. Methods Appl. Mech. Eng.*, 298:121–158, jan 2016.

- [27] Paladim, D.A., Moitinho de Almeida, J.P., Bordas, S.P.A., and Kerfriden, P., Guaranteed error bounds in homogenisation: an optimum stochastic approach to preserve the numerical separation of scales, *Int. J. Numer. Methods Eng.*, 110(2):103–132, apr 2017.
- [28] Collins, J.B., Estep, D., and Tavener, S.J., A posteriori error estimation for a cut cell finite volume method with uncertain interface location, *Int. J. Uncertain. Quantif.*, pp. 415–432, 2015.
- [29] Zaccardi, C., Chamoin, L., Cottureau, R., and Dhia, H.B., Error estimation and model adaptation for a stochastic-deterministic coupling method based on the Arlequin method, *Int. J. Numer. Methods Eng.*, 96(2):87–109, 2013.
- [30] Giles, M.B., Multilevel Monte Carlo methods, *Acta Numer.*, 24(May):259–328, 2015.
- [31] Haji-Ali, A.L., Nobile, F., von Schwerin, E., and Tempone, R., Optimization of mesh hierarchies in multilevel monte carlo samplers, *Stochastics Partial Differ. Equations Anal. Comput.*, 4(1):76–112, 2016.
- [32] Li, C. and Der Kiureghian, A., Optimal discretization of random fields, *J. Eng. Mech.*, 119(6):1136–1154, jun 1993.
- [33] Der Kiureghian, A. and Ke, J.B., The stochastic finite element method in structural reliability, *Probabilistic Eng. Mech.*, 3(2):83–91, jun 1988.
- [34] Zeldin, B.A. and Spanos, P.D., On random field discretization in stochastic finite elements, *J. Appl. Mech.*, 65(2):320, 1998.
- [35] Eigel, M., Merdon, C., and Neumann, J., An adaptive multilevel monte carlo method with stochastic bounds for quantities of interest with uncertain data, *SIAM-ASA J. Uncertain. Quantif.*, 4(1):1219–1245, 2016.
- [36] Bonilla-Villalba, P., Error estimation and adaptivity for finite element structural dynamics models under parameter uncertainty, PhD thesis, Cardiff University, 2018.
- [37] Doebling, S.W., Farrar, C.R., and Prime, M.B., A summary review of vibration-based damage identification methods, *Shock Vib. Dig.*, 30(2):91–105, 1998.
- [38] Steele, C., The Probability Distribution of the Elastic Properties of Pure Metals, *Appl. Math.*, 05(06):898–903, 2014.
- [39] Ladeveze, P. and Leguillon, D., Error Estimate Procedure in the Finite Element Method and Applications, *SIAM J. Numer. Anal.*, 20(3):485–509, 1983.
- [40] González-Estrada, O.A., Nadal, E., Ródenas, J.J., Kerfriden, P., Bordas, S.P.P.A.P.A.P.A., and Fuenmayor, F.J., Mesh adaptivity driven by goal-oriented locally equilibrated superconvergent patch recovery, *Comput. Mech.*, 53(5):957–976, 2014.
- [41] Zienkiewicz, O.C. and Zhu, J.Z., A simple error estimator and adaptive procedure for practical engineering analysis, *Int. J. Numer. Methods Eng.*, 24(2):337–357, 1987.
- [42] Babuška, I. and Rheinboldt, W.C., A-posteriori error estimates for the finite element method, *Int. J. Numer. Methods Eng.*, 12(10):1597–1615, 1978.
- [43] Babuška, I. and Rheinboldt, W.C., Error Estimates for Adaptive Finite Element Computations, *SIAM J. Numer. Anal.*, 15(4):736–754, aug 1978.
- [44] Becker, R. and Rannacher, R., A feed-back approach to error control in finite element methods: Basic Analysis and Examples, *East-West J. Numer.*, 4:237–264, 1996.
- [45] Cirak, F. and Ramm, E., A posteriori error estimation and adaptivity for linear elasticity using the reciprocal theorem, *Comput. Methods Appl. Mech. Eng.*, 156(1-4):351–362, apr 1998.

- [46] Oden, J.T. and Prudhomme, S., Goal-oriented error estimation and adaptivity for the finite element method, *Comput. Math. with Appl.*, 41(5-6):735–756, 2001.
- [47] Robert, C.P. and Casella, G., *Monte Carlo Statistical Methods*, Springer New York, 2004.
- [48] Gentle, J., *Random Number Generation and Monte Carlo Methods*, Statistics and Computing, Springer-Verlag, New York, 2 edition, 2003.
- [49] Rubinstein, R.Y. and Kroese, D.P., *Simulation and the Monte Carlo Method*, Wiley Series in Probability and Statistics, John Wiley & Sons, Inc., Hoboken, NJ, USA, 2 edition, dec 2007.
- [50] Nobile, F., Tempone, R., and Webster, C.G., A Sparse Grid Stochastic Collocation Method for Partial Differential Equations with Random Input Data, *SIAM J. Numer. Anal.*, 46(5):2309–2345, jan 2008.
- [51] Barthelmann, V., Novak, E., and Ritter, K., High dimensional polynomial interpolation on sparse grids, *Adv. Comput. Math.*, 12(4):273–288, may 2000.
- [52] Melchers, R.E., Importance sampling in structural systems, *Struct. Saf.*, 6(1):3–10, 1989.
- [53] Gilks, W.R., Richardson, S., and Spiegelhalter, D.J., *Markov Chain Monte Carlo in Practise*, Chapman and Hall/CRC, 1995.
- [54] Cotter, S.L., Dashti, M., and Stuart, A.M., Approximation of Bayesian Inverse Problems for PDEs, *SIAM J. Numer. Anal.*, 48(1):322–345, jan 2010.
- [55] Stuart, A.M., Inverse problems: A Bayesian perspective, *Acta Numer.*, 19(5):451–559, may 2010.
- [56] Evensen, G., The Ensemble Kalman Filter: theoretical formulation and practical implementation, *Ocean Dyn.*, 53(4):343–367, nov 2003.
- [57] Neyman, J., Outline of a Theory of Statistical Estimation Based on the Classical Theory of Probability, *Philos. Trans. R. Soc. A Math. Phys. Eng. Sci.*, 236(767):333–380, aug 1937.
- [58] Evans, D.H., An Application of Numerical Integration Techniques to Statistical Tolerancing, II: A Note on the Error, *Technometrics*, 13(2):315, may 1971.
- [59] Seo, H.S. and Kwak, B.M., Efficient statistical tolerance analysis for general distributions using three-point information, *Int. J. Prod. Res.*, 40(4):931–944, 2002.
- [60] Lee, S.H. and Chen, W., A comparative study of uncertainty propagation methods for black-box type functions, *Proc. Asme Int. Des. Eng. Tech. Conf. Comput. Inf. Eng. Conf. 2007, Vol 6, Pts a B*, 6B(847):1275–1284, 2008.
- [61] Parés, N. and Diez, P., A new equilibrated residual method improving accuracy and efficiency of flux-free error estimates, *Comput. Methods Appl. Mech. Eng.*, 313:785–816, 2017.
- [62] Efron, B., Bootstrap Methods: Another Look at the Jackknife, *Ann. Stat.*, (1):1–26, jan 1979.
- [63] van der Vaart, A.W. *Bootstrap*, pp. 326–340. Cambridge Series in Statistical and Probabilistic Mathematics. Cambridge University Press, 1998.
- [64] Rognes, M.E. and Logg, A., Automated Goal-Oriented Error Control I: Stationary Variational Problems, *SIAM J. Sci. Comput.*, 35(3):C173–C193, jan 2013.
- [65] Geuzaine, C. and Remacle, J.F., Gmsh: A 3-D finite element mesh generator with built-in pre- and post-processing facilities, *Int. J. Numer. Methods Eng.*, 79(11):1309–1331, 2009.